Simulating flow behavior of soft particles in a quasi-two-dimensional silo under varying gravity

by

Abigail Tadlock

A thesis submitted to the Department of Physics
in partial fulfillment of the
requirements for the Degree of
Bachelor of Arts in Physics

May 21, 2023

Approved by

Kerstin Nordstrom, Associate Professor, Department of Physics, Mount Holyoke College
Spencer Smith, Associate Professor, Department of Physics, Mount Holyoke College
Jessica Sidman, Professor of Mathematics on the John Stewart Kennedy Foundation, Mount Holyoke College

ABSTRACT

Systems as diverse as sand, crowds of people, and the rings of Saturn can be classified as granular materials. Omnipresent in our daily lives, in nearly every field of science, and part of billions of dollars per year in industry, we know surprisingly little about how granular materials behave. For systems such as gases we can take the understanding that atoms will bounce off of each other and the walls and derive the Ideal Gas Law. No such local behavior to bulk behavior scaling exists for granular materials. Due to factors discussed within such as unequal force distribution, there is a mid-"meso-scale present that disrupts our ability to predict bulk behavior. As a result, granular systems can behave both in a liquid-like manner when they flow or a solid-like manner when they jam.

In this thesis, we study the specific geometry of a silo, which can be simply conceptualized as a container, filled with a granular material, that has a outlet (aperture) in the bottom – thus allowing the grains to flow out under the force of gravity. This ostensibly simple system is reasonably well described by an equation called the Beverloo equation, but only for typical systems: hard particles at regular Earth gravity ($9.81m/s^2$). Understanding how systems of soft particles flow is important for building a comprehensive model of granular flow and for applications in fields such as biology. Understanding how granular materials behave in different gravity is essential for space exploration and extraplanetary science. For example, if we want to land a spacecraft on an asteroid that has its own microgravity, we need to understand how the grains that make up the surface of that asteroid will behave in a system very different to what we have on Earth.

In order to study these questions, we use molecular dynamics (MD) simulations through the software LAMMPS (Large Atomic/Molecular Massively Parallel Simulator). This software uses Newton's law of motion and a model of particle contact to output position, velocity, and force data for each particle at every timestep. Simulating our system allows us to easily vary particle stiffness, gravity, and the diameter of the aperture. We study a quasi-two-dimensional system made up of a single vertical layer of spheres. We present our results on local measurements such as granular temperature, mesoscale measurements such as velocity profiles, and bulk measurements such as flow rate. We also discuss pressure waves that we observed within our system. We present a hypothesis for a relationship between granular temperature and deviation from the Beverloo equation. We also observe that a dimensionless ratio of gravity and stiffness, Γ, collapses many of our measurements and reveals trends.

ACKNOWLEDGMENTS

First, I want to thank my advisor Kerstin Nordstrom for her guidance and mentorship during the multiple years of this project. You've been a fantastic mentor who supported me when I was first starting this project as a first-year during the COVID summer, which was such a challenging time. Over the years I've become increasingly confident in my research skills thanks to you. As I prepare to go to graduate school next year I feel confident in my ability to take a research question and imagine how I could explore it, which is a testament to your mentorship skills and an incredible takeaway from my undergraduate research.

I also want to thank Spencer Smith and Jessica Sidman for taking time out of their busy schedules to complete my thesis committee. Spencer, you've been an absolutely incredible professor of the many physics classes I've taken with you. Thank you as well for your sage academic advising advice.

A special thanks to Anna Maria Moran, my lab mate and fellow physics thesis writer. This thing would not have been finished without our countless writing and editing sessions. I also want to thank my fellow 2023 physics seniors and next-year roommates: Anna Maria (again), Lucy Sternberg, Kat Fraser, and Lyds Johnson. You've made some challenging classes and semesters bearable and I can't wait for our adventures in Boston next year. The wider physics department has been an incredibly supportive environment for the last four years and leaving it behind is a bittersweet moment. But I'll always have the sweater I knitted in-between note taking in 315 and 325 to remind me of my time here.

Special shout out to Loryn Engelbrecht, the incredible department coordinator. The department would not be able to function without you coordinating conference travel, food for events, room reservations, and countless other things I'm not even aware of. Nothing brightens my day like the snacks and treats at physics events (donuts with faculty especially), and we have you to thank for coordinating all of it.

Last but certainly not least, I need to thank my parents. You've supported me throughout my college years, listing to my venting and celebrating about anything and everything. I love you both so much. ♡

TABLE OF CONTENTS

LIST OF FIGURES

1 INTRODUCTION

Granular materials are ubiquitous and the study of them spans many disciplines, from physics and astronomy to biology, geology, and more. A granular material is simply a collection of discrete, macroscopic particles. Obvious everyday granular materials include sand and trail mix, but there are also less obvious, or more exotic, granular materials like the rings of Saturn or crowds of pedestrians. They also include both hard systems, such as gravel, and soft systems, such as oil droplets suspended in water or blood cells suspended in plasma. Particles in a granular system interact simply via contact forces, such as friction and normal forces. Additionally, the particle size is large enough that thermal motions are negligible. Systems of very small molecules, such as gases, are governed primarily by random motion, referred to as thermal motion. Granular systems have large enough particles that these random motions are not a contributing factor to the energy of the system (although a similar concept, called granular temperature will be discussed in section 2.5.2) [1]. Because of their ubiquity, there are many motivations for understanding granular materials. For instance, after water, granular materials are the most used material in industry, with wide-ranging manufacturing applications [2].

Granular systems are made up of many discrete particles, each of which interacts with neighboring particles. Despite the conceptual simplicity of these systems, the collective interactions of these particles produce rich phenomena which are still poorly understood. For ideal gases, one can use classical kinetic theory to predict the bulk properties of gases simply by modeling the microscopic interactions as elastic collisions. For pure fluids, other

statistical physics arguments predict bulk properties like viscosity, and simple force and energy arguments can give us predictive equations of fluid motion. For granular materials, similar attempts fail — bulk behavior cannot be predicted by microscopic interactions alone — there appear to be multiple length scales that govern material properties [3]. As a result, granular systems can be studied at multiple scales, including the microscale, that of individual particles, the “mesoscale" (middle scale), local collections of particles, and the bulk scale, that of the system as a whole [4]. Microscale interactions include friction and other contact forces between particles and forces between particles and the wall. Mesoscale observations include force chains, the phenomenon that particles do not share equal loads of force, but instead force propagates in “chains" (see figure 1.1 throughout the material. Bulk scale observations include flow rate, one of the main focuses of this research.

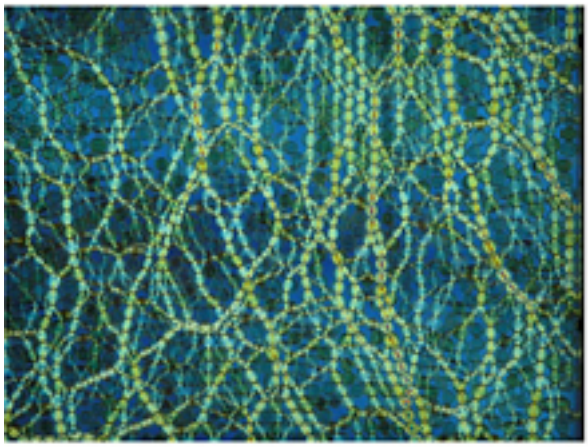

Figure 1.1: Example of force chains, from Behringer *et al.* [5]. The light colored chains show uneven stress distribution within the material.

In 1895, German scientist H. Janssen published a paper describing the results of a series of experiments analyzing the pressure at the bottom of a corn silo. Traditional silos

could hold up to a 25 m tall layer of corn – the equivalent of 250 tons. Janssen reasoned that there must be enormous pressure on the walls and floor of the silo and ran a series of smaller experiments, which led to a surprising conclusion. When the height of the corn layer exceeded the width of the silo, the pressure at the bottom saturated and ceased to increase [6]. One of the most important aspects of granular materials in a silo is this effect, called the Janssen effect, which is the result of the nature of granular materials. There are contact forces both between particles and static friction between particles and the walls [1]. The frictional particles support shear forces, which means that the force chains propagate not only downwards, as expected, but also horizontally. This creates load-bearing structures across the silo, allowing the pressure to saturate at the bottom. The Janssen effect causes granular materials flowing from a silo to behave remarkably differently from fluid flow.

If you fill a container with fluid, the pressure at the bottom is proportional to the height of the fluid in the container. The flow of water from the bottom decreases as the height of the fluid decreases. However, with granular materials, due to the Janssen effect, the flow rate of the granular particles out of the orifice is relatively constant.

The flow of fluids is described by the Navier-Stokes equations. These equations are derived from the existing theory of fluids and how they behave. The set of equations fully describes the observed experimental behavior. No equations analogous to Navier-Stokes exist for the flow of granular materials. The Beverloo equation is a formula for granular flow. Derived from experimental observations and dimensional analysis rather than a theoretical basis, the Beverloo equation is empirical and requires fitting to each individual system [7]. This will be discussed in further detail in the next chapter. Although

it has been proven to be accurate for most systems, it tends to underestimate the flow rate of soft particles. Due to their ability to deform, soft particles can essentially squeeze through an outlet in a way hard particles cannot [8]. Furthermore, the effects of gravity on granular flow have not been well quantified. The Beverloo equation states that the flow rate should scale with the square root of gravity, but few experiments have tested this [9]. Non-normal gravity is understandably difficult to study experimentally. Past experiments have used centrifuges to increase gravity [9], tilted the silo of near-frictionless particles to decrease effective gravity [8], and rotated a single layer of particles to decrease effective gravity [10]. Understanding how gravity, especially low gravity, affects granular materials is important to fields such as planetary science and systems in microgravity, like the surface of asteroids or motion within asteroid belts. Microgravity here refers to systems where gravity is a fraction of Earth's gravity.

In this work, we use simulations of soft granular flow to explore the applicability of Beverloo to systems of soft particles in varying levels of gravity. We systematically vary the width of the outlet aperture of the silo, the stiffness of the particles, and the gravity of the system.

2 BACKGROUND

As explained previously, there is no complete theory for how different systems of granular materials will behave. Granular materials are relevant to fields of science as diverse as mechanical engineering, planetary science, geology, and astrophysics. Due to the diversity of applications, it is important to understand how these omnipresent materials behave in unusual environments, such as microgravity. The previous chapter explored the general background of granular materials. This chapter will explore the relevant mechanics of granular materials in more detail as well as the behaviors that we will study in this thesis.

We perform molecular dynamics (MD) simulations using software called LAMMPS (Large-scale Atomic/Molecular Massively Parallel Simulator) ([11]) to explore the flow behavior of particles. We vary three main parameters: 1) silo outlet diameter, 2) particle stiffness, and 3) gravity. We assume a uniform gravitational field that mimics the constant gravity on planetary surfaces. We aim to quantify a relationship between micro- and mesoscale flow behavior and the gravity and stiffness of particles, represented by a dimensionless measurement we will introduce in Chapter 3.

2.1. System Geometry

This research concerns granular particles within a silo geometry. This can be thought of as a container with an outlet (hole) at the bottom, allowing particles to flow out. We choose to use a silo because it is a standard geometry that is simple yet poorly understood [12]. Silos also have many practical applications, including transporting granular materials in industry (e.g. sand for concrete, animal feed, pharmaceutical powders, and pills). In

this context, they are prone to issues like clogging and ratholing, which is when only the material directly above the outlet moves and the material on the edges does not move.

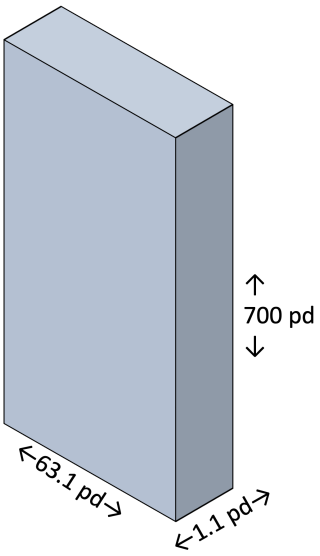

Figure 2.1: Diagram of the quasi-2D silo used for simulations. Side lengths are given in particle diameters (pd). Not to scale.

We specifically utilize a quasi-two-dimensional geometry. “Quasi-2D" refers to how the system consists of a single 2D layer of particles, but the particles are 3D spheres. The quasi-2D geometry allows us to more easily visualize the behavior of individual particles. Because all particles within the system can be visualized at the same time, analysis is easier. Furthermore, while LAMMPS can simulate true 3D systems, they are more computationally intensive than quasi-2D systems. Quasi-2D systems are frequently used in silo flow research and serve as analogues to 3D systems [8, 13, 14]. Examples of real-life 2D systems include traffic, pedestrian flow, and material flow on a conveyor belt.

The simulation box consists of a single vertical layer of spherical particles within a 62 particle diameter (pd) wide and 700 pd tall box. The depth of the box is 1.1 pd, thus allowing only one layer of spherical particles, creating the quasi-two-dimensional nature.

These dimensions were chosen to minimize the effects of the walls on the flow. Previous studies [7, 15] have found that the flow rate out of a silo is independent of the diameter of the silo if the diameter is greater than $2.5D_0$, where D_0 is the outlet diameter and if the silo diameter is also greater than D_0+30 pd Our system satisfies both of these requirements as the maximum outlet diameter used is 20 pd.

2.2. Jamming

Granular systems can exhibit solid-like and fluid-like behaviors. In the solid-like state the system is considered to be “jammed". Compare sand in two states: flowing liquid-like from your hand and packed into a sand castle. The sand castle is an example of a jammed state caused by confining the particles with pressure. In the same way, granular systems in a silo may jam as particles attempt to exit the outlet [12].

2.2.1 Clogging

Clogging is a specific jamming situation where the unidirectional flow causes a jammed state and the flow is blocked by particles. In a 2D geometry this is caused by particles forming an arch over the outlet. Hard spherical particles form symmetric, spherical arches. The range of outlet diameters at which clogs appear varies depending on the system. It is still debated whether there is a “critical diameter" size above which the system will never clog, or whether clogging just becomes statistically unlikely. However, recent computational and experimental studies agree with the second theory that there is no critical outlet size

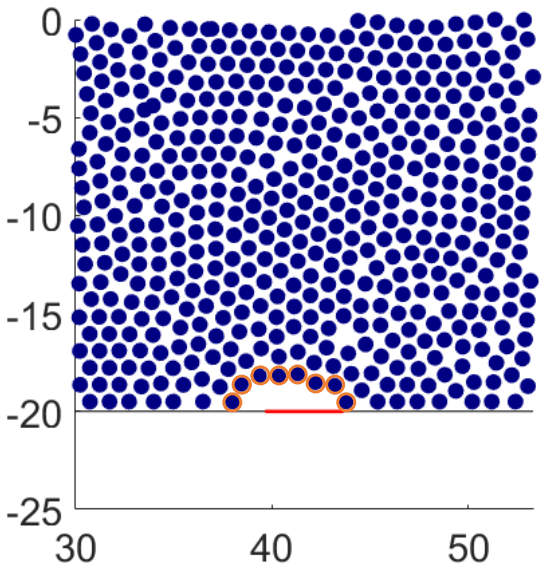

Figure 2.2: An example of a clog from one of our experiments. Outlet diameter (red line) is 4 pd. Due to soft particles, low gravity, and friction the arch is not symmetric about the outlet, nor a perfect semicircle.

[16, 17]. This thesis does not examine clogging; however, we do explore behavior changes as outlet diameter approaches a diameter at which clogging occurs. Figure 2.2 shows an example of a clog from one of our simulations. We found that our system clogged in simulations with an outlet diameter of less than 5 particle diameters wide. Our observed arch in a softer, lower gravity system is neither symmetric nor spherical. While beyond the scope of this thesis, investigating these arch shapes could be future work. We study only systems that do not clog, with an outlet diameter of 6 pd or larger.

2.3. Flow

As introduced in the previous chapter, the silo flow rate of grains is constant as long as certain conditions are fulfilled. The particle stack must be 1.2 times the diameter of the silo [7]. Figure 2.3 shows an example psuedo image of what our system looks like

when flowing. First proposed by Beverloo et al. in 1961, the Beverloo equation (2.1) empirically describes this constant flow rate [18]. It functions based on the argument that there is an “arch" spanning and proportional in size to the outlet diameter. Below this arch, the particles are in free fall, and above this arch their velocities are negligible. It should be noted that this is a non-rigorous explanation and that there is some disagreement on this [19]. The Beverloo Equation is:

$$W = C\rho_b\sqrt{g}(D_0 - kp_d)^{n+1/2} \tag{2.1}$$

In this equation, the flow rate W scales with the square root of gravity, g. It also depends on the diameter of the outlet aperture, D_0, bulk density ρ_d and particle diameter p_b. Dimensional analysis of this system gives a $D_0^{3/2}$ relationship for a two-dimensional system and $D_0^{5/2}$ for a three-dimensional system, so $n = 1$ for 2D (or quasi-2D) systems and $n = 2$ for 3D systems [7]. C and k are dimensionless empirical fitting constants that must be scaled for each system. C is an empirical discharge coefficient and depends on the friction coefficient and the bulk density of the system. A typical fitted C value for a hard, frictional system is between 0.55 and 0.65 [7]. k, the shape coefficient, is more inscrutable and there is a debate about its meaning and a reasonable range of values for it. One argument is that it relates to the effective outlet size and the self-blocking of the particles. Some papers say that k is independent of particle size and between 1 and 2 [15], while other papers found that the only reasonable value is 1 [20].

Because this research concerns soft particles, it is important to note that particle stiffness, or Young’s modulus E, does not appear explicitly within this equation. Rather, it is implied in the bulk density ρ_b term.

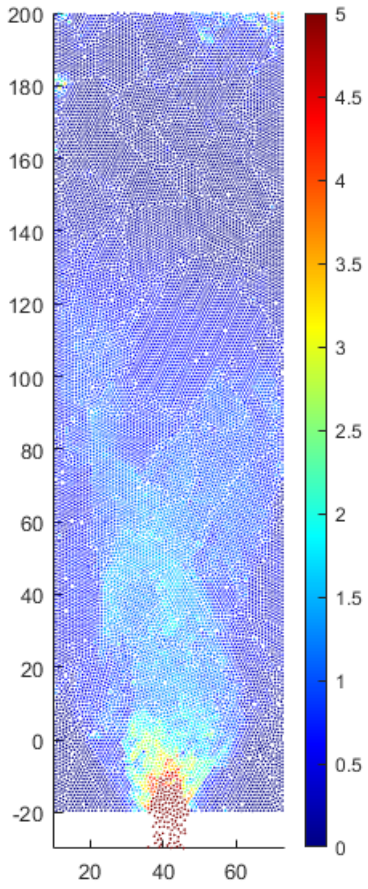

Figure 2.3: An example pseudo image of our system, colored by instantaneous speed. Simulation parameters: $E = 10^7$ Pa, $g = 1$g, $D_0 = 11$ pd.

$$\rho_b = \frac{mN_{particles}}{V_{total}} \tag{2.2}$$

In equation 2.2, ρ_b is calculated by dividing the number of particles by the total volume they take up, including the spaces between particles (2.2) . As particles become softer, they deform and compress more under their own weight, leading to an increase in ρ_b [7].

Although Beverloo is relatively accurate in describing many systems, it falls short in a few key ways. It was developed for very specific systems of hard particles flowing under normal Earth gravity through relatively small outlet diameters. When a system diverges from one of these measurements, the fit results in less accurate predictions. Furthermore, Beverloo assumes a monodisperse system, a system in which all particles have the same diameter. Most real granular systems are bidisperse (containing particles of two diameters) or polydisperse (containing particles of three or more diameters). However, because this research concerns a monodisperse system, we will not further explore this topic.

The next issue concerns the two empirical constants, C and k. There is no clear theory for what gives rise to these constants, besides their connections to flow rate and particle shape. While it is relatively easy to fit C by taking flow measurements for different outlet diameters, one must fit it to each system individually. k is often assumed to be 1, and some previous work has suggested eliminating k entirely [7]. Furthermore, while fitting C and k for a small range of outlet sizes results in a close correlation with Beverloo, for experiments spanning several decades of particle diameters the fit is no longer accurate, diverging at either small or large apertures, depending on the fit [7].

Finally, previous work in soft systems and systems flowing at non-normal gravity have shown divergence from Beverloo. Because soft particles have the ability to deform,

they often flow at higher rates than predicted by Beverloo. This is especially true near the clogging point, as soft particles are able to deform in order to pass through outlets smaller than their diameter [8].

2.4. Soft Particles

In our simulations we model particles with Young's moduli ("stiffness") between 10^4 - 10^7 Pa. The softest particles are similar to hydrogel beads used in previous studies, such as Hong *et al.* (2017) [8]. Soft particles have the ability to deform, which often leads to significantly different behaviors from otherwise identical systems of hard particles.

For example, as mentioned in the previous section, clogging diameter is smaller for softer systems because soft particles are able to deform. This often causes Beverloo to significantly diverge from measured flow rate for large outlets [8]. Importantly, recent research found that friction plays a key role in the flow of soft granular systems. Pongó *et al.* (2021) found that for soft granular systems with relatively high friction maintained a steady flow regardless of particle layer height, but low-friction systems behaved similarly to a fluid and flow rate decreased with layer height [21]. Low friction particles can slide past each other, but high friction particles become jammed, which causes a constant flow rate. We simulate soft particles with friction ($\mu_f = 0.5$), discussed more in Chapter 3. Because our systems are frictional, we found a constant flow rate that did not vary with fill height.

2.5. Measurements

Chapter 3 describes the LAMMPS Molecular Dynamics (MD) simulations performed. The output of these simulations is a file containing position, velocity, and force information for every single particle (identified by a particle ID) for each timestep. These data

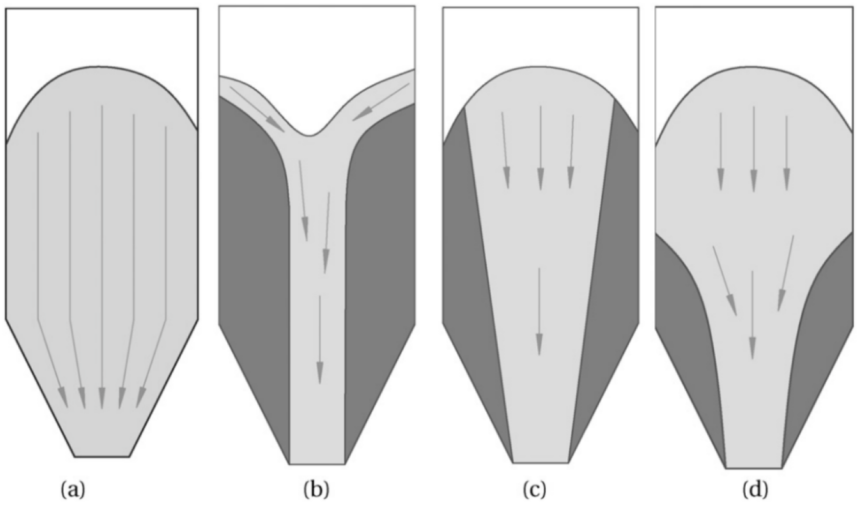

Figure 2.4: Examples of different flow patterns a) Bulk, all particles move downwards, including particles on the walls. flow b-d) Types of Funnel Flow. Only particles above the outlet are moving downwards and particles on the edges are static. Figure from Mathews *et al.* (2016) [9].

can be used to calculate several different measurements of flow. The simulation updates in timesteps of 0.1 milliseconds and data is recorded every 1000 of these timesteps, for a data resolution of 10 samples/s. A typical simulation has 100 seconds, or 1000 samples, of data.

2.5.1 Velocity Profile

Several different flow patterns are possible within a silo. All the material can be flowing downwards in what is commonly referred to as “mass flow", but which we will call “bulk flow" to avoid confusion with the measurement of flow rate in kg/s. Bulk flow is generally considered ideal; however, it is more common to have some form of funnel flow in which particles on the edge of the silo do not move due to shear forces from the walls [9]. Figure 2.4 shows different possible flow patterns.

One method of determining the flow pattern of a silo is through a velocity profile. This is a time average of particle velocity at a given vertical height, or between a range of heights. The velocity is calculated for each horizontal position. Experimentally this is calculated using high-resolution video and particle tracking. We easily calculate this, discussed in-depth in section 4.1, using the output position and velocity data. In an ideal bulk flow pattern, the vertical velocity profile would be a flat line. In a funnel flow pattern, the vertical velocity profile will have a u-shape or v-shape depending on how slowly the edge particles are moving compared to the center particles.

2.5.2 Granular Temperature

During granular flow, the bulk movement is downwards towards the outlet but individual particle movements may vary from this. Much like a gas has thermal motion, “granular temperature", first introduced by Ogawa *et al.* in 1980 [22], is a measure of fluctuations in a granular system. It is caused by particle-particle collisions and the resulting random motion in the system [23]. In our simulations, we find the time average of the granular temperature near the outlet using the x-component of the velocity (see Chapter 4 for more details), using equation (2.3), from Endo *et al.* (2018) [14].

$$T_{gx} \sim \langle \delta V_x^2 \rangle = \langle (V_x - \langle V_x \rangle)^2 \rangle \tag{2.3}$$

This equation presents the granular temperature T_{gx} as the variance of the horizontal component of the velocity, $\langle \delta V_x^2 \rangle$. Variance is the average squared deviation of the data from the mean. Endo *et al.* (2018) studied a similar silo system so we imitate their tactic of ignoring the vertical motion. By only considering the horizontal fluctuations we ignore

the complication of having to subtract out the directed vertical motion. Because the system is driven by gravity, the directed motion is in the vertical direction. The deviation from this vertical direction is the observed random motion.

2.5.3 Pressure Waves

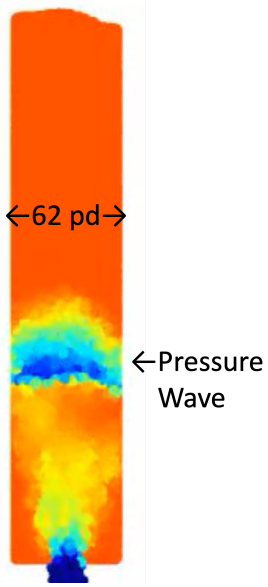

Figure 2.5: Pressure wave within one of our simulations. The colors represent vertical velocity, with blue being regions of high downwards velocity. The pressure waves move upwards in the silo, but the constituent particles have a high downwards velocity.

A phenomenon observed within silos in both laboratory and industrial applications is pressure or stress waves (hereafter referred to as pressure waves). These waves are comprised of traveling energy within the silo. The waves are a traveling disturbance, not a bulk movement of particles. It is particularly important to understand pressure waves in granular materials because they can place unexpected stresses on silos [24]. Similar pressure waves are also observed in crowds of people [25, 26] and fluidized rod systems [27].

However, this behavior has not been well studied because of measurement difficulties. One theory of the cause of pressure waves is stick-slip interactions between particles and the silo walls [24]. Stick-slip interactions occur when an object has a high static friction and thus moves along a surface in a “jerky" motion, where it “sticks" on the surface until the force exceed the static friction and then it “slips" and jerks forward.

We identify pressure waves (figure 2.5) in our simulations by examining both local density and velocity (see chapter 4 for full method). The waves travel upward within the silo, although the velocity of the constituent particles is strongly downward. The waves also have a lower density than the surrounding material. We observed pressure waves in all of our simulations, though they were less frequent and slower in softer systems (see chapter 5 for in-depth discussion). Pressure waves can be described by the generic wave equation $c = f\lambda$, where c is the wave speed, f is the frequency and λ is the wave length.

3 LAMMPS SIMULATION DESIGN

Simulating granular flow allows us to easily vary conditions that are difficult to experimentally alter, such as gravity. Experimental methods to change gravity do exist, such as a geophysical centrifuge [9] to artificially increase gravity. The angle of the silo can be altered, artificially decreasing gravity [8]. However, this method creates more friction with the walls of the silo, so it is not a true analogue and works best for systems with very low friction. Simulations can complement and expand the experimental results. Molecular dynamics (MD) simulations in particular are useful because they contain models for many different types of condensed matter, including molecules, crystals, and discrete particles.

Many body systems in condensed matter are governed by the same laws of physics as other fields, but solving them by conventional means is extremely difficult as they have many degrees of freedom and contain numerous individual particles. Even systems with only three particles are often not analytically solveable. Simulations simplify and significantly speed up this process. Simply stated, a MD simulation takes basic laws of motion and force and uses them to calculate how a large multiparticle system will behave. For each timestep of the simulation, the force on each simulated atom is calculated and its position and velocity are updated. The boundaries of the system are encoded along with forces such as gravity and frictional forces. Such simulations are computationally intensive because of the combination of a massive number of timesteps, often in the millions or billions, combined with a large number of simulated atoms.

LAMMPS (Large-scale Atomic/Molecular Massively Parallel Simulator) is a MD program originally created and maintained by Sandia National Labs, written in C++. We use LAMMPS to model granular silo flow. The output position and velocity data allow us to study the mechanics of the system. Because changing system characteristics like gravity is as simple as altering a single line of code, this allows us to easily study systems that are difficult, if not impossible, to explore experimentally.

3.1. The Simulation Box

The simulation space in LAMMPS is created using a “fix region" command. This creates a simulation box with defined walls that particles interact with in specifiable ways. There are two main regions in our simulation: the silo and the larger box that holds the silo. Particles interact with the silo walls via the contact forces discussed in the next section. The larger simulation box has periodic boundaries on the left and right. An escaped particle, exiting the left side of the simulation box, will re-enter on the right with the same direction and velocity. Particles sometimes escape when the simulated forces are so great that the simulation “loses track" of due to the length of the timestep. As a result, these particles end up expelled from the simulation box. This typically happens to less than 500 particles per simulation, or around 1.5% of the total. The bottom boundary, which particles leaving the aperture will hit, is fixed.

We create the exit aperture in the simulation by creating a third region, the same size as the hopper but with an exit aperture, and merging it with the original hopper, thus creating an outlet for particles to flow out. Section 3.4 discusses in-depth how we insert particles into the region.

3.2. Contact Forces

LAMMPS has two methods in the granular package to calculate the force resulting from particles in contact with each other. The two methods (or “styles") are Hookean (with sub-styles that include history force or do not include history) and Hertzian (which always includes history). Here, “history" refers to the tangential shear force (3.4). This force includes a term that accounts for the tangential displacement during the contact period, thus the history of the particle interaction [28].

We use a Hertzian model for simuating the contact forces between particles. This is an alteration to the Hookean model of particle interaction. Both of these models assume that when the the distance, r between two particles of radius R_i and R_j is greater than the contact distance, $d = R_i + R_j$, there is no contact force between the particles. The Hookean model assumes a linear force response with overlap, whereas the Hertzian model modifies the Hookean model so that the force response is dependent on overlap area, and therefore non-linear. The Hertzian model accounts for particle size in this way, but the Hookean model does not. As a result, the Hookean model would require adding additional mathematical complications for a polydisperse system.

3.2.1 Hookean and Hertzian Models of Contact Forces

The Hookean model of particle contact assumes that when particles overlap (are squished together) the overlap area functions similarly to a spring. The Hookean Model for the force between two particles that are in contact is the sum of the normal force between the two particles and the tangential force between them. These two forces are themselves the

sum of additional forces. The normal force is composed of a static contact force, $\vec{F_c}$, and a dynamic damping force $\vec{F_{dn}}$.

$$\vec{F_c} = k_n \delta \hat{n}_{ij} \tag{3.1}$$

$$\vec{F}_{dn} = m_{eff} \gamma_n \vec{v}_n \tag{3.2}$$

The contact force is proportional to the overlap between the particles, symbolized by $\delta = d - r$, the elastic constant for normal contact k_n, which can be thought of as a linear spring constant, and the unit vector of the line connecting the center of the two particles, $\hat{n}_{ij}$ (equation (3.1)). Essentially, this says that the more overlap particles have (the more they are “squished together"), the greater the normal force. The damping force portion of the normal force is proportional to the particles effective mass $m_{eff} = \frac{M_i M_j}{M_i + M_j}$, the relative velocity between the two particles in the normal direction $\vec{v}_n$, and the viscoelastic damping constant for normal contact γ_n, which is related (and sometimes equal) to the coefficient of restitution. The coefficient of restitution can be thought of as the “bounciness" of an object.

The tangential force describes how the particles are moving parallel to each other. Like the normal force, it consists of two terms, a shear force F_s and a tangential damping force F_{dt}.

$$\vec{F}_{dt} = m_{eff} \gamma_t \vec{v}_t \tag{3.3}$$

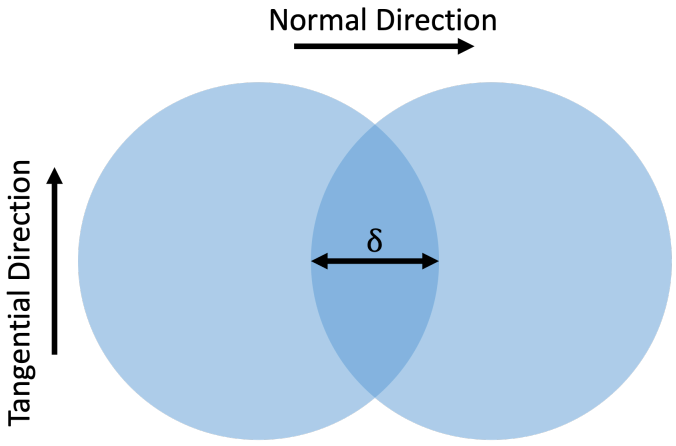

Figure 3.1: This diagram shows two particles with overlap distance δ. The normal direction is the direction of the line that connects the center of the two particles. The tangential direction is perpendicular to the normal direction.

$$\vec{F}_s = k_t \Delta \vec{s}_t \tag{3.4}$$

The tangential damping force (3.3) is identical to the normal damping force, except that the viscoelastic damping constant is different, γ_t and we consider the velocity in the tangential direction $\vec{v}_t$. The shear force (3.4) is the “history term" that contains information about the tangential displacement over the period of contact

The total force between particles can now be given by taking the vector sum of all of the normal and shear forces.

$$\vec{F}_{hk} = \vec{F}_N + \vec{F}_T = (\vec{F}_c - \vec{F}_{dn}) - (\vec{F}_s + \vec{F}_{dt})$$

$$\vec{F}_{hk} = (k_n \delta \hat{n}_{ij} - m_{eff} \gamma_n \vec{v}_n) - (k_t \Delta \vec{s}_t + m_{eff} \gamma_t \vec{v}_t) \tag{3.5}$$

The Hertzian force equation is a modification of the Hookean force equation (3.5). For a monodisperse system, such as the one we simulate, this prefix is a constant $\sqrt{\frac{R}{2}}$.

$$\vec{F}_{hz} = \sqrt{\delta}\sqrt{\frac{R_i R_j}{R_i + R_j}}\vec{F}_{hk} = \sqrt{\delta}\sqrt{\frac{R}{2}}\vec{F}_{hk}$$

$$\vec{F}_{hz} = \sqrt{\frac{\delta R}{2}}((k_n \delta \hat{n}_{ij} - m_{eff}\gamma_n \vec{v}_n) - (k_t \Delta \vec{s}_t + m_{eff}\gamma_t \vec{v}_t)) \tag{3.6}$$

Now, the constants k_n and k_t are no longer linear spring constants, but now non-linear spring constants with units of force/area. These are given by equations 3.7 and 3.8.

$$k_n = \frac{4G}{3(1-\nu)} = \frac{2E}{3(1-\nu^2)} \tag{3.7}$$

$$k_t = \frac{4G}{2-\nu} = \frac{E}{(2-\nu)(1+\nu)} \tag{3.8}$$

Here ν is the Poisson ratio, a measure of how a material deforms when subjected to stress, and G is the shear modulus and is given by $G = \frac{E}{2(1+\nu)}$, where E is Young's modulus, particle stiffness [29].

Table 3.1 contains the values for the constants in our simulation. Values for k_n and k_t are calculated using equations 3.7-8. γ_n and γ_t are calculated using (3.9) and (3.10), where a is given by (3.11).

$$\gamma_n = \sqrt{\frac{2ak_n}{m(1+0.25a)}} \tag{3.9}$$

Gravity (g)	0.1g - 20g
Radius (R)	1
Mass (m)	1
Coefficient of friction (μ_f)	0.5
Coefficient of restitution	0.66
Poisson's ratio (ν)	$\frac{2}{7}$
Young's Modulus (E)	10^4-10^7

Table 3.1: Simulation Contants

$$\gamma_t = 0.5\gamma_n = 0.5\sqrt{\frac{2ak_n}{m(1+0.25a)}} \tag{3.10}$$

$$a = -2\log^2(\frac{0.66}{\pi}) \tag{3.11}$$

3.2.2 Other Contact Forces

LAMMPS also governs how particles interact with the simulated silo walls. We use the same Hertzian force relationship as for particle interactions. Friction with the walls is also included. Some granular systems include cohesive forces that cause particles to stick together. We do not consider these forces in our modeling.

3.3. Phase Space

Our simulations use a single layer of monodisperse spherical particles within a quasi-2D silo. We systematically vary three elements of the simulation: gravity, elastic modulus, and outlet diameter. Gravity is varied between 0.1 and 20 times Earth's gravity, the elastic modulus is varied between 10^4-10^7 Pa, and the outlet diameter is varied between 6 and 20

times the particle diameter. Although the simulations do use SI units, values should still be considered relative simulation units. For example, as shown in table 3.1, the radius of the particles is 1 m, which is not a real-world value.

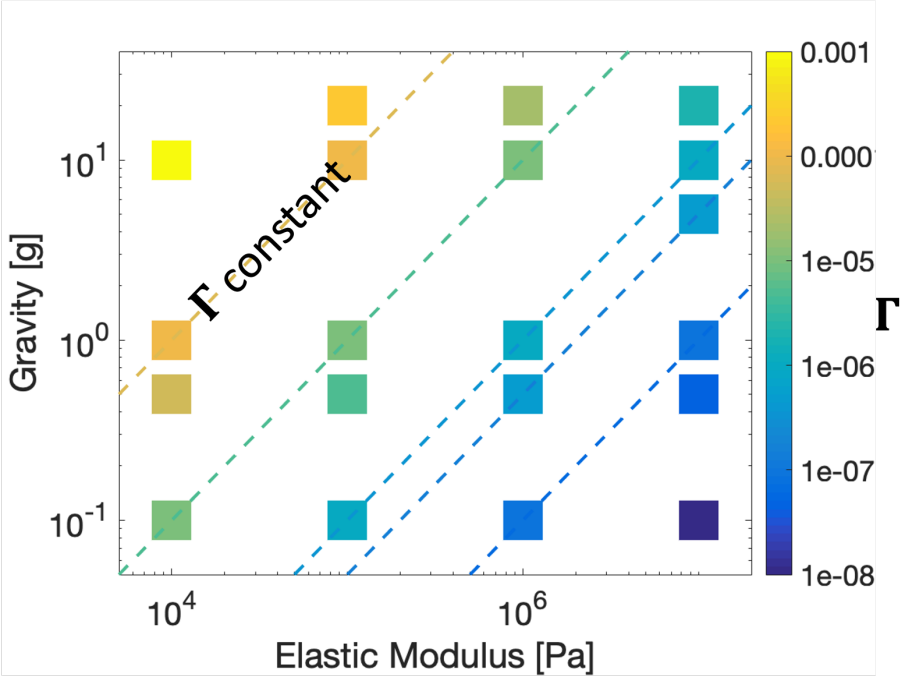

Figure 3.2: Simulation Phase Space. Each point also has the outlet diameter varied between 6 and 20 pd. Γ is constant along the dashed lines.

Figure 3.2 shows the phase space of our simulations. Each of the markers represents a set of simulations with a set gravity and elastic modulus and varying outlet diameter. We derive a dimensionless constant Γ to navigate within this phase space and compare different simulations.

$$\Gamma = \frac{\rho g}{p_d E} \tag{3.12}$$

Γ is a relation between particle density ρ derived from the known mass and radius, the gravity of the system g, the particle diameter p_d, and the elastic modulus E. Due to our simulation units, we treat Γ as a simple ratio of gravity and particle stiffness. Within figure 3.2, the dashed lines show simulations with the same values of Γ. Normalizing measurements by Γ reveals underlying trends in many of our measurements, detailed in chapter 4.

3.4. Simulation Design

The silo is flat bottomed with a width of 63.3 pd and a depth of 1.1 pd. We use the create_atoms LAMMPS command to insert particles into the silo. All of the particles are created at once, located at random positions with random velocities within the silo, and allowed to settle. This creates a highly random packing structure, in contrast to the more crystalline packing structure found when particles are “poured" into the system by generating them at a height (see figure 3.4). When the particles are poured into the silo, they will settle into a hexagonal close packing structure, shown in figure 3.3. With the random generation method, this crystalline packing is not present. The more crystalline the system, the more likely it is to clog due to the regular arrangement of particles. As a result, this filling dependent randomness is a benefit. Furthermore, 3D monodisperse systems do not crystallize, making this method a better approximation.

This alternate filling method was chosen to eliminate the significant period of time necessary to generate 30,000 particles using the pouring method. The create_atoms command includes a random seed, which is used to randomly generate the initial positions and velocities. One consequence of the create_atoms filling method is that unless this random seed is varied, simulations run with the same gravitational and stiffness parameters will

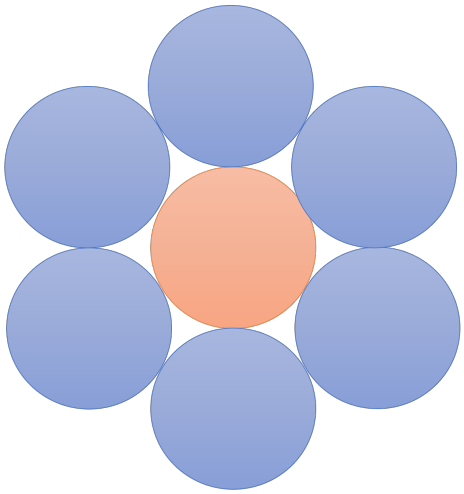

Figure 3.3: Hexagonal close packing.

have identical packing. We did not vary the seed, so this was true for our simulations. This allows us certainty that variations due to outlet diameter are not due to varying levels of crystallinity in the packing structure. In the future, varying the seed might allow us to test different packing structures.

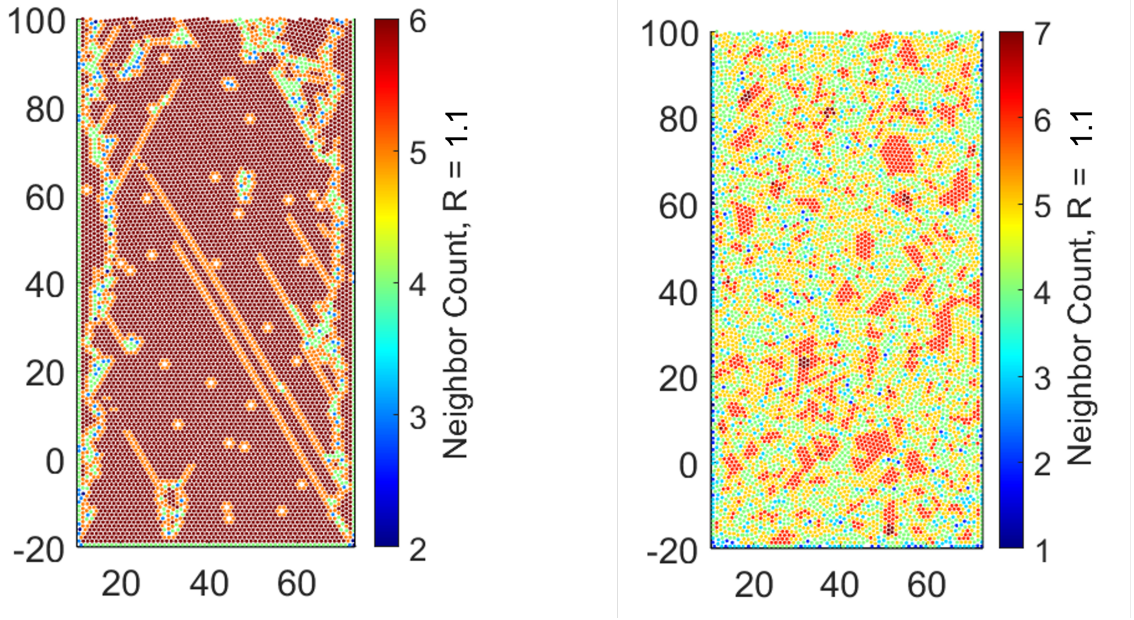

(a) Pouring Method

(b) Random Creation Method

Figure 3.4: Packing structure dependence on filling method. (a) pouring filling method (b) particle creation filling method. The colors correspond to neighbor count. The poured method creates near uniform crystalline packing (6 neighbors, dark red), with small crystalline defects along the edges and in the middle. The randomly generated system is predominantly 4 neighbors and non-crystalline.

4 KEY MEASUREMENTS

4.1. Velocity Profiles

As discussed in section 2.5.1, velocity profiles give insight into the flow pattern. This is a measurement of whether the material is engaged in bulk flow or some variation of tunnel flow.

4.1.1 Measurement

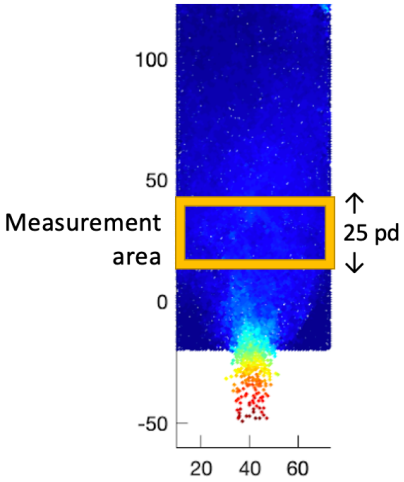

Figure 4.1: Measurement area for the velocity profiles. The velocity of particles within the box at each horizontal point are time-averaged over the period of steady flow.

Our measurement method is based on the method used by Mathews *et al.* (2016) [9]. We define a measurement box spanning the width of the silo and 25 pd tall, beginning 30 pd above the bottom of the silo and ending 60 pd above the outlet (see fig. 4.1). At each

horizontal point, the vertical velocity of particles within the box is time-averaged over the period of steady flow.

4.1.2 Results

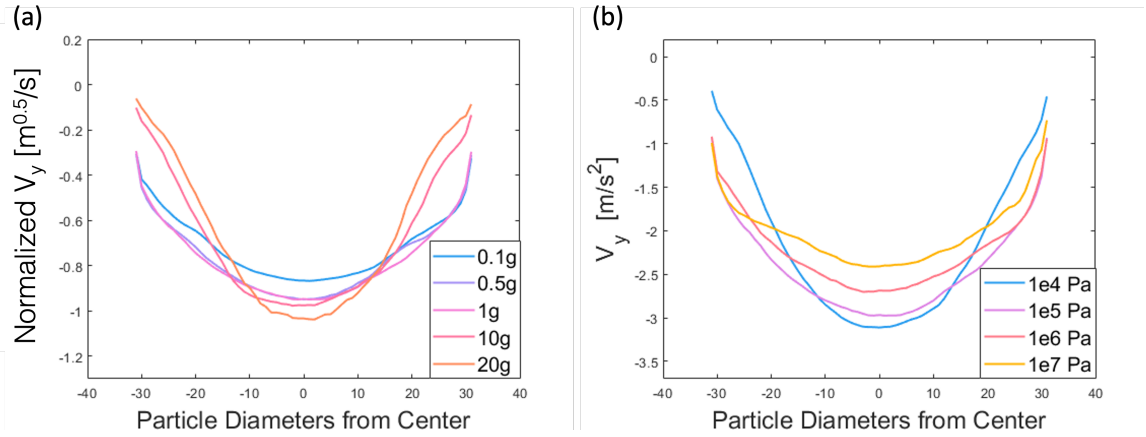

Figure 4.2: Velocity profiles for (a) constant Elastic Modulus ($E = 10^5$ Pa), varying gravity (b) constant gravity ($g = 1$ g), varying stiffness. The x-axis is particle diameters from the center of the silo.

We found velocity profiles for each of our 20 pd outlet diameter simulations. We compared the profiles by plotting ones of constant stiffness or gravity against each other (figure 4.2 shows examples). In these diagrams we see that the profiles shift from a “u"-shape to a “v"-shape. This tells us that as we increase gravity or decrease stiffness, the system is flowing more in a tunnel-like way. The particles above the outlet are flowing quickly, but the particles at the walls are flowing at rates very close to 0 m/s. In contrast, harder systems and systems with lower gravity are closer to bulk flow, with the velocity of particles on the wall much more similar to that of particles in the center.

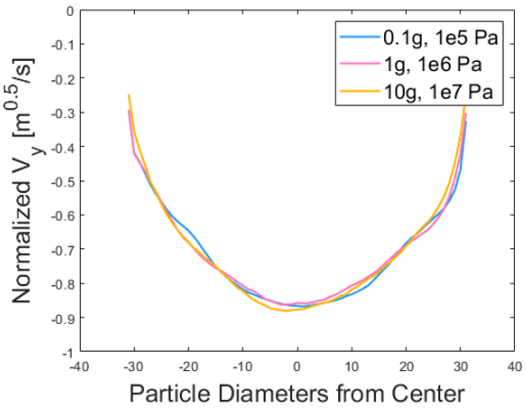

Figure 4.3: Velocity profiles for constant Γ.

Because we see the same trend in shape with both varying gravity and stiffness, we compare the velocity profiles for systems with the same value of Γ. Figure 4.3 shows the results for this. Here, the shapes have collapsed. This tells us that Γ has the power to reveal the underlying trends in the data.

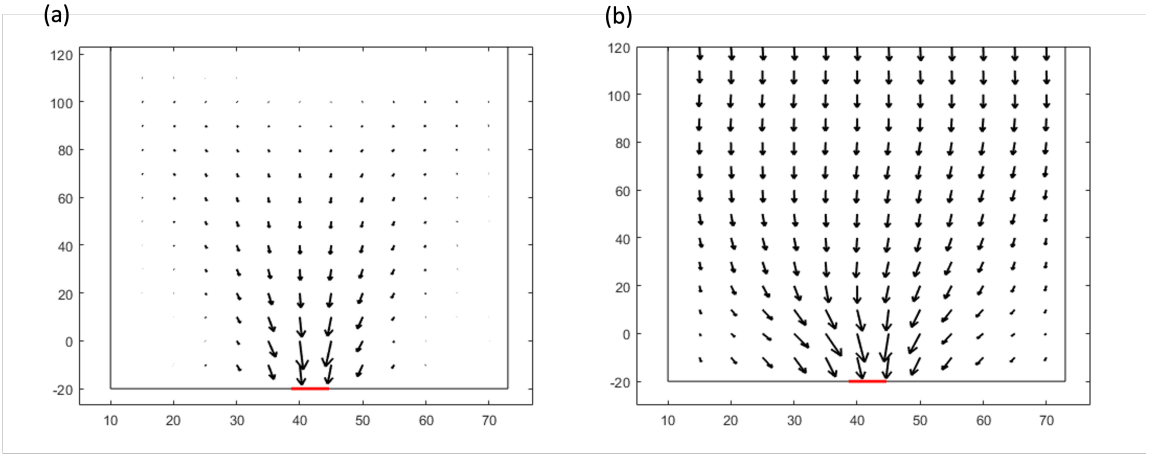

Figure 4.4: Flow Profiles for (a) high Γ ($g = 10$g, $E = 10^4$Pa) and (b) low Γ ($g = 0.1$g, $E = 10^7$Pa). The vector field shows the direction and magnitude of the flow. The red line marks the location of the outlet.

We also generated flow profiles for some of our systems. These use a vector field to show the direction and magnitude of the flow. Figure 4.4 confirms what we learned from the velocity profiles. High Γ systems show tunneling behavior, whereas low Γ systems are closer to bulk flow. Previous studies found similar tunneling behavior in frictionless systems [30] and granular fluid systems [31]. This suggests that our high Γ systems are behaving in a more fluid-like manner than the low Γ systems, which behave more as a solid.

4.2. Granular Temperature

Described in detail in section 2.5.2, granular temperature is a measure of random motion in the system. We have defined this as the variance of the horizontal velocity (2.3), because this is deviation from the bulk downwards behavior.

4.2.1 Measurement

We measure the granular temperature in a box centered on the outlet with a width of $D_0 + 10$ pd, where D_0 is the outlet diameter (figure 4.5). The box is 50 pd tall. This was chosen because 50 pd is the height at which the outlet-noise-dominated region ends and other flow characteristics, like pressure waves (Chapter 5), become distinct and difficult to average over. We consider as many timesteps as possible, while the particle layer is taller than the 50 pd tall measurement box.

4.2.2 Results

We normalize the granular temperature data by gravity. All data analysis in this section was performed with the normalized data. Gravity is the primary driving force of the system's

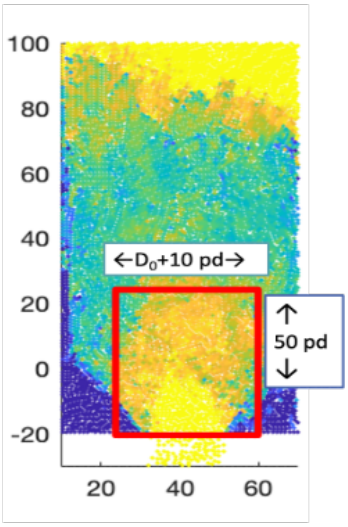

Figure 4.5: The measurement area for granular temperature. It is centered around the outlet with a width equal to the outlet diameter plus 10 pd and a height of 50 pd.

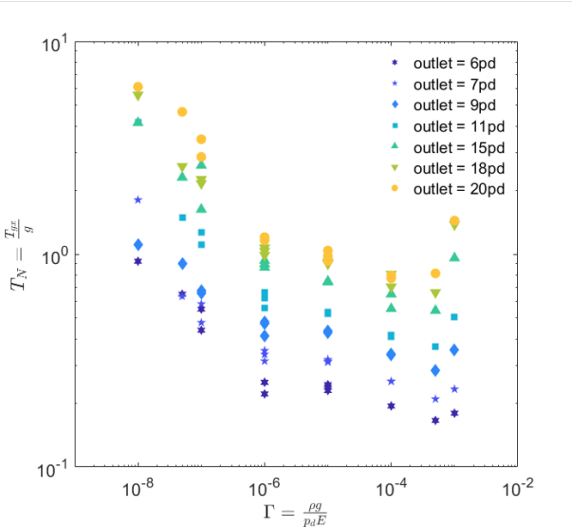

Figure 4.6: Granular temperature, normalized by gravity, plotted against Γ.

motion; therefore, the characteristic speed of the system is proportional to the square root of gravity. As a result, $T_{gx} \propto v^2 \propto g$. Figure 4.6 shows the resultant normalized granular temperature plotted against Γ. There is significant dependence on outlet diameter in these

results. When we keep Γ constant and look at the dependence on D_0, we see that there is a linear relationship with D_0 (figure 4.7(a)) and linear fits are performed. We looked for trends in the intercepts to determine whether a trend indicated a critical aperture, but there is no clear trend (see figure 4.7(b)). However, the slopes decrease with Γ. This suggests that the amount of random motion in softer, higher gravity systems is less dependent on outlet diameter.

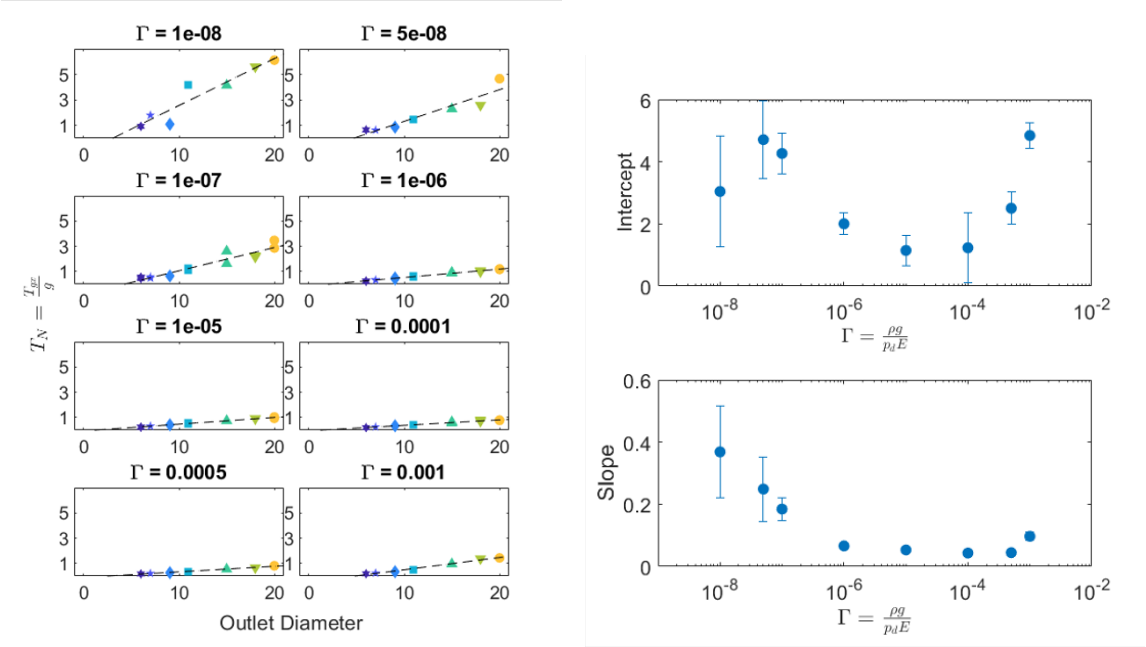

(a) Granular temperature vs Outlet Diameter

(b) Slopes and intercepts of linear fits

Figure 4.7: (a) Granular temperature plotted against outlet diameter for different values of Γ with linear fits. (b) The slopes and intercepts of the linear fits.

Figure 4.8 shows the overall trend with with both outlet diameter and Γ. The system "cools down" as the outlet diameter decreases and as Γ increases. At first, this may seem counter-intuitive because there is actually more movement happening at higher Γ because gravity is greater. This result shows that the motion is more directed at higher Γ. Although

the particles move faster, their random motion is smaller, resulting in a lower granular temperature. The implications of this result are discussed more in-depth in Chapter 6.

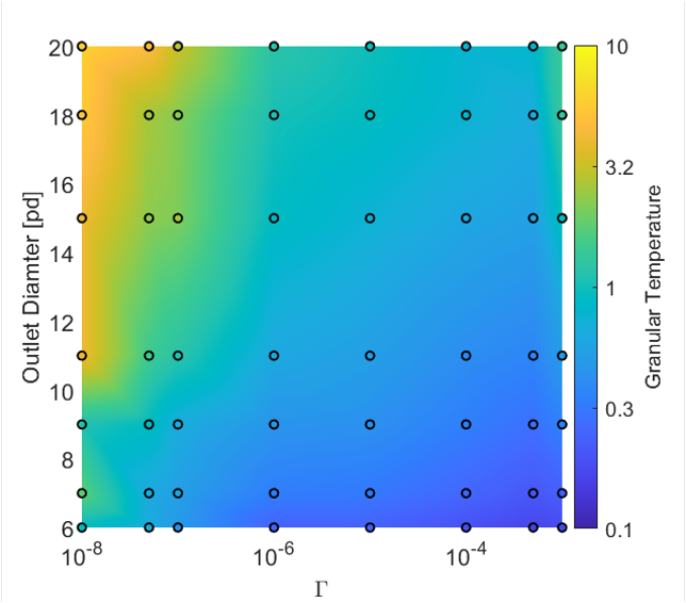

Figure 4.8: A contour plot of granular temperature. The black circles are data points and the colored background is interpolation between data points.

4.3. Flow Rate

As discussed in Section 2.3, the flow rate from a silo is constant due to pressure saturation at the bottom. In this section, we discuss our method for measuring flow rate, our comparison to the Beverloo prediction, and our potential explanations for the deviation from the prediction.

4.3.1 Measurement

We measure the flow rate in our system by counting the particles (identified by their simulation particle identification number) that fall below the outlet ($y = -20$) at each timestep.

We then add the data for 10 time steps to convert them to particles per second. In order to convert to mass flow we multiply by the mass of the particles, given by the equation $m = \rho V = 4.188$ kg.

4.3.2 Comparison to Beverloo prediction

We find that the flow rate of our system is relatively constant, outside of small random fluctuations. Figure 4.9 shows an example of the mass flow over time of one of our systems (parameters: $g = 10$ g, $E = 10^7$ Pa, $D_0 = 20$ pd). The sharp drop off is when there is no longer enough particles in the system to sustain the Janssen Effect. Refer back to Chapter 1 for more information on the geometry necessary for this.

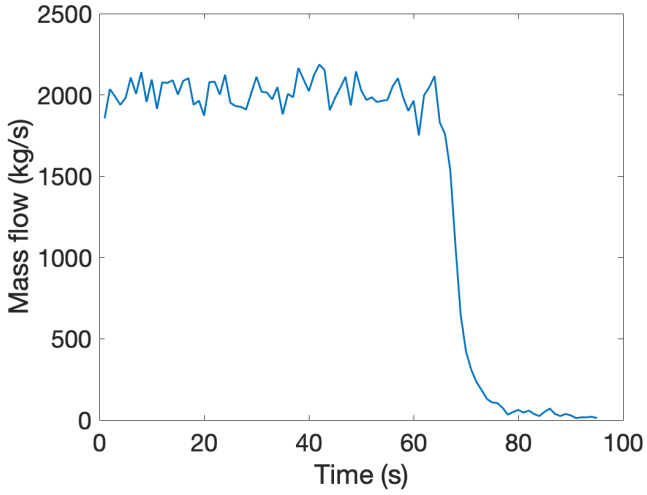

Figure 4.9: Example graph of time vs mass flow from the $g = 10$ g, $E = 10^7$ Pa, $D_0 = 20$ pd simulation. The flow is relatively constant (2021 $\pm$ 85 kg/s) until there are only approximately 7,000 particles remaining (23% of the original), at which point it sharply drops off.

We calculate the average flow rate during the steady-flow period for each of our simulations. Figure 4.10 shows our results, normalized by $\sqrt{g}$ to better allow comparison. We then fit the Beverloo equation $W/\sqrt{g} = C\rho_b(D_0 - kd_p)^{3/2}$ using $k = 1$, $C = 0.6$, and $\rho_b = 4.25$ kg/m^3. We choose one Beverloo fit to compare to our simulation runs instead of fitting each run individually because we are interested in exploring how our systems differ from a hard particle fit. The value for ρ_b changed depending on the system, but 4.25 was the hard particle limit for the least amount of deformation under the weight of the particle stack. The value for C was calculated by fitting each simulation run for a given g and E individually, then taking the average C value. The values of C and p_b for every simulation are located in a data table in the appendices.

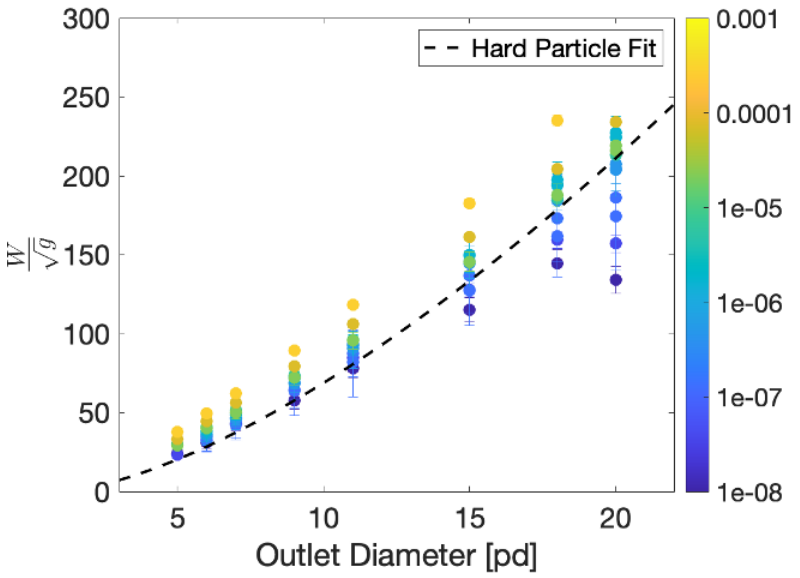

Figure 4.10: Flow rate data plotted against a hard particle Beverloo fit ($C = 0.6$, $\rho_b = 4.25$ kg/m^3, $k = 1$). The colors represent Γ. Yellow is soft particles and high gravity, blue is hard particles and lower gravity.

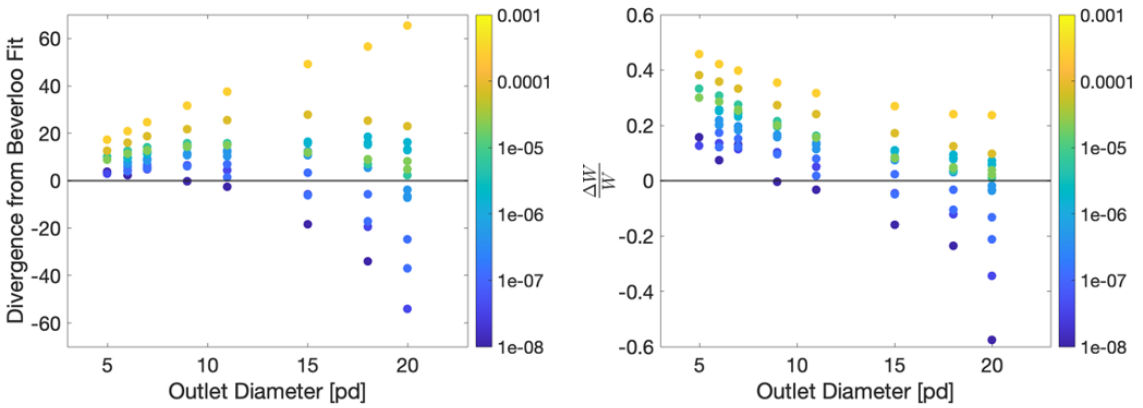

(a) Absolute divergence from the Beverloo fit (black line).

(b) Divergence from the Beverloo fit, normalized by mass flow rate.

Figure 4.11: Absolute and normalized divergence from the Beverloo fit. The color scale is Γ.

Figure 4.11(a) shows the absolute deviation from the Beverloo fit. We see that for small outlet diameters Beverloo consistently underestimates the true flow rate. As the diameter of the outlet increases, it continues to underestimate the flow rate for high Γ systems (soft particles and high gravity), but begins to overestimate the flow rate for low Γ systems (harder particles and low gravity). Figure 4.11(b) shows the deviation normalized by flow rate, giving a percentage deviation. Note the significant 60% deviation from Beverloo for hard particles in low gravity. As mentioned previously, this is simultaneously **one of the most important areas of granular materials to study in the early stages of space exploration** and extra-planetary science and one of the least explored parts of the gravity-stiffness phase space due to the difficulty of simulating lower gravity experimentally.

4.3.3 Correlation with Granular Temperature

We observe a potential correlation between the deviation from the Beverloo prediction and the observed granular temperature near the outlet. Figure 4.12 shows that systems with high Γ have a lower granular temperature and are underestimated by Beverloo. Low Γ systems have a higher granular temperature and are overestimated by Beverloo. To further explore this trend, we directly plot the flow rate, the absolute deviation from Beverloo fit, and the normalized deviation from the Beverloo fit against the granular temperature (figure 4.13).

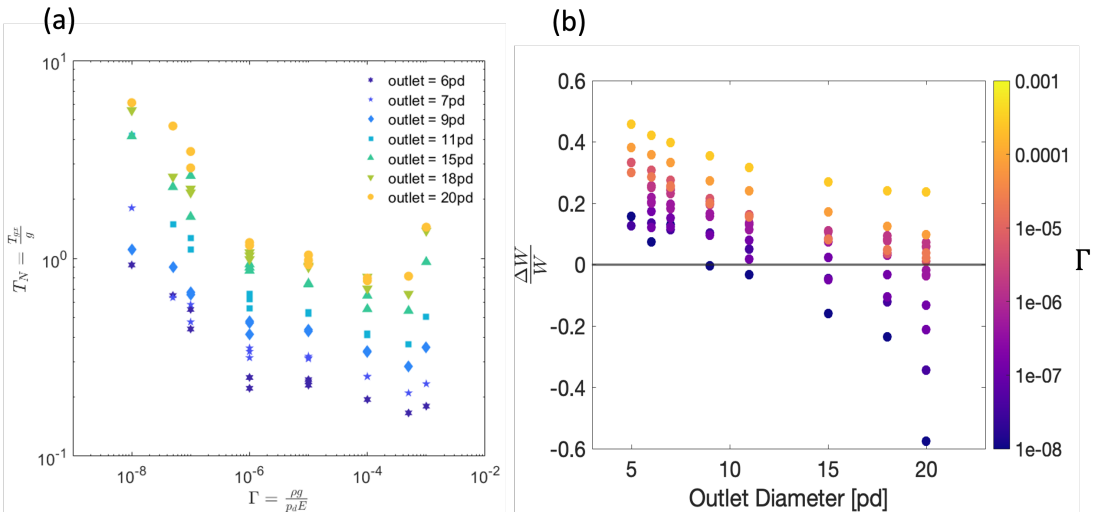

Figure 4.12: Comparison of (a) Γ vs. granular temperature (b) Outlet diameter vs. normalized deviation from Beverloo fit. High Γ systems have a lower granular temperature and are underestimated by Beverloo. Low Γ systems have a higher granular temperature and are overestimated by Beverloo.

All three of these graphs reveal a correlation between flow rate and normalized granular temperature. Normalized granular temperature is proportional to $\delta v_x^2/v^2$, which is of the same order of magnitude as the flow rate deviations, allowing for the comparison. As

the granular temperature increases, the flow rate decreases and the deviation from Beverloo becomes negative. The outlying data set - dark red in 4.13(a), yellow in (b) and (c) - is the suite of simulations $E = 10^4$ Pa, $g = 10$ g. Because this system is subject to such extreme forces due to the combination of the very soft particles and high gravity, it is frequently the outlying trend in data comparisons.

One possible explanation for this correlation is the strength of the driving force of the system. High Γ systems have very strong downward driving forces due to their high gravity and softness. It is possible that this stronger driving force results in less horizontal motion near the outlet. This decreased horizontal motion may be one of the mechanisms behind the Beverloo underprediction for these data. Vice versa, the low Γ systems have a lower gravity and harder particles, potentially leading to more horizontal movement and a higher granular temperature and a mechanism behind the Beverloo overprediction. Another possible explanation is that the the increased softness of particles is effectively an increase in friction. For two particles in contact and subject to the same forces, the softer particles will have a greater overlap distance. Discussed in section **??**, both the normal force (related to friction), and the frictional shear force scale with overlap distance, δ. This results in an increased effective frictional force. This may allows the particles to move alongside each other increasing flow rate, whereas harder systems are more likely to move against each other, decreasing flow rate.

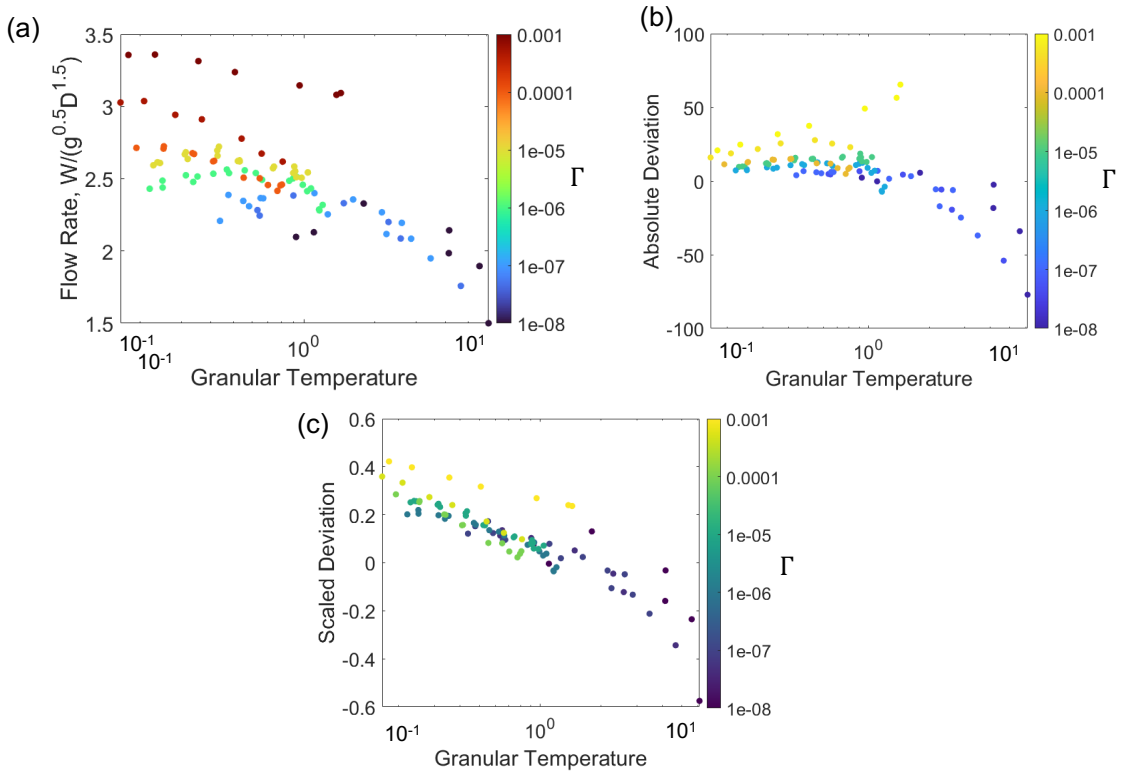

Figure 4.13: The colors for all graphs represent outlet diameter. (a) The flow rate plotted against the granular temperature, normalized by outlet diameter $D_0^{1.5}$ and gravity $\sqrt{g}$ (b) The divergence from Beverloo, normalized by absolute flow rate plotted against the granular temperature. (c) The absolute divergence from Beverloo plotted against the granular temperature.

5 PRESSURE WAVES

In this section we will present our findings on the pressure waves within our system (figure 5.1). These waves travel upwards in the silo, opposite the direction of flow. Interestingly, they are made up of particles that are moving downwards, opposite the wave direction. The waves also have a lower density than the surrounding particles. The following section outlines how we analyze these waves.

As discussed in section 2.5.3, pressure waves can place unexpected stresses on a silo, so it is important to understand their origin and behavior. Furthermore, we are interested in exploring whether there is a link between the flow rate or fluctuations and the pressure waves. Even if no link is found, pressure waves have implications for data processing. For example, we encountered issues in trying to take the granular temperature of the entire silo because the pressure waves caused our measurements to vary significantly depending on the timescale. Other data measurements that rely on time averages could run into a similar issue in a system with pressure waves, especially if the waves have a low frequency or velocity and thus are more prominent on the time-average.

5.1. Method of Analysis

Our goal in analyzing pressure waves is to determine how they impact the flow. We visualize the pressure waves within the silo by creating a spacetime diagram. We calculate this by averaging the measurement of interest (velocity, etc.) above the outlet at each horizontal position up to the top of the silo for a given timestep. This measurement becomes

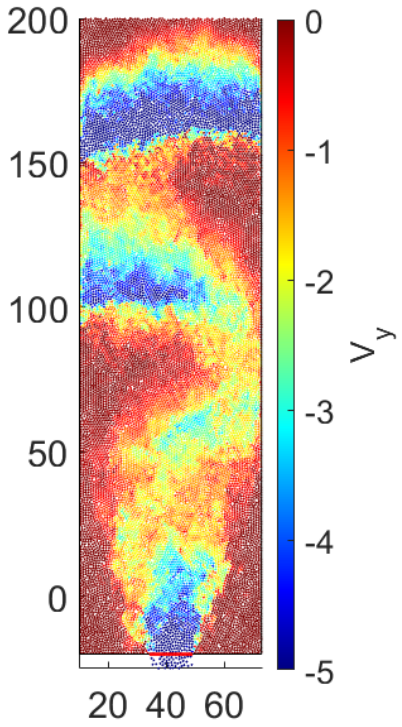

Figure 5.1: Pseudoimage of one of our simulations ($g = 1$ g, $D_0 = 15$ pd, $E = 10^4$ Pa). The colorscale is vertical velocity. The dark blue “bubbles" are the pressure waves. They travel upwards even though the constituent particles are moving down at high velocity. The waves also have a lower density than the surrounding particles (visible from the blank white spots in the blue regions).

one column of pixels in the spacetime diagram. The pressure waves appear as diagonal traces on the diagram.

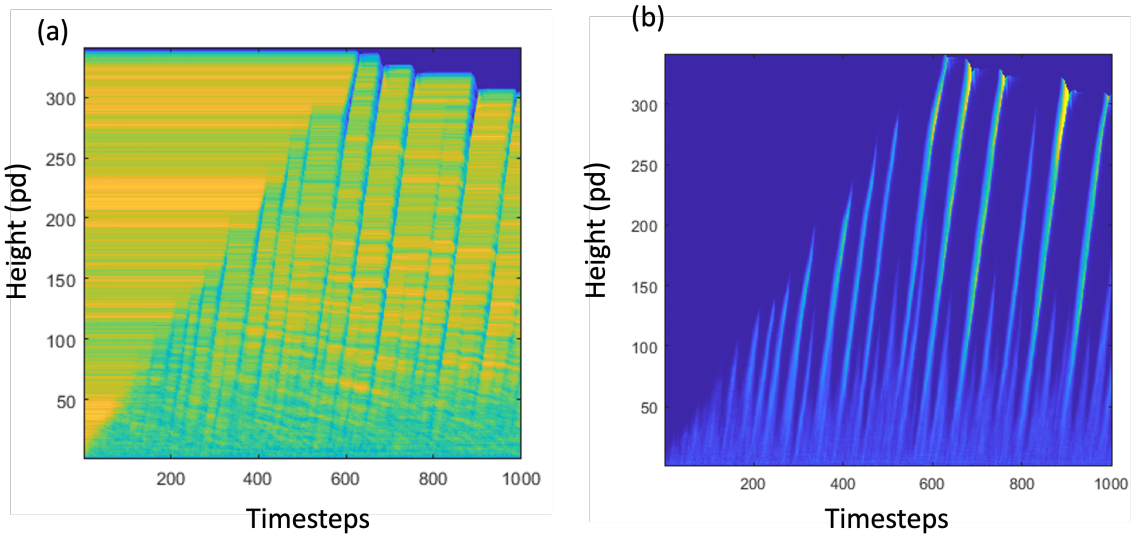

Figure 5.2: (a) Spacetime diagram showing local neighbor count. The initial neighbor count varies with vertical position and particles exit the silo and the particle stack decreases, horizontal bands are formed. These make analysis difficult. (b) Spacetime diagram showing speed. The pressure waves are much clearer as the stationary particles are uniform.

Most previous research concerning pressure waves uses local variations in density in order to track the waves [24, 26, 27]. However, figure 5.2 compares the diagrams for the local neighbor count with a radius of 2 particle diameters (a proxy for local density) and speed. The particle packing is random and noncrystalline particles have different numbers of local neighbors. As the silo empties and the particle layer height decreases, these local packing differences remain relatively constant until they are disturbed by a pressure wave. Figure 5.3 shows an example of how the packing structure can remain unchanged over time. This results in horizontal bands of different density appearing in

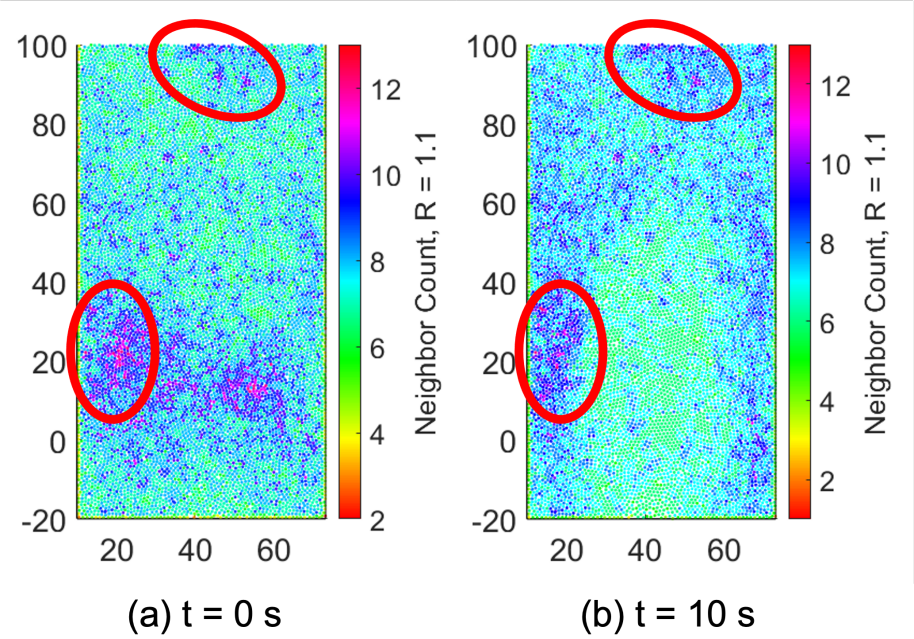

Figure 5.3: Neighbor count with a radius of 1.1 pd at (a) t = 0s and (b) t = 10s for $g = 10$ g, $D_0 = 15$ pd, and $E = 10^4$ Pa. The light teal region of lower density in (b) shows the region disturbed by the pressure waves. Notice that the same packing structure is apparent in the regions untouched by the pressure waves (red circles).

the spacetime diagram, which made analysis significantly more difficult. On the contrary, these particles unaffected by either the outlet motion or the pressure waves all have the same negligible speeds. As a result, using speed for the space time diagram produces significantly easier to process images.

From the spacetime diagrams we can calculate the wave speed c, frequency f, and length λ. The slope of the wave lines is equal to the wave speed. The time between wave peaks moving horizontally across the diagram can be used to determine the frequency. The wave length can then be calculated from these two measurements $\lambda = \frac{c}{f}$. We extract these measurements in MATLAB by taking a horizontal slice of the silo (figure 5.6 is an example).

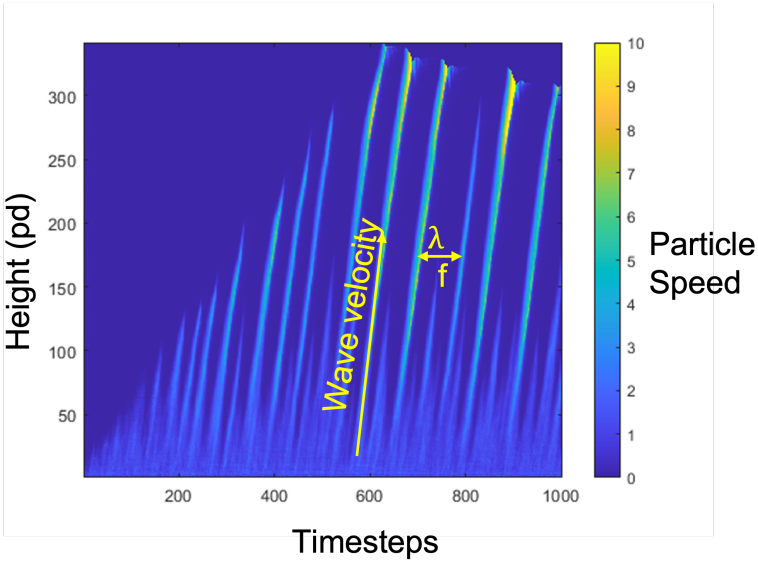

Figure 5.4: An example speed spacetime diagram of a system with pressure waves (not the same system as figure 5.1). The waves are the lines of high speed. The slope of the line is the velocity of the wave and the separation gives both frequency and wavelength.

The spikes in speed on the graph are the waves as they pass that height. The “find-peaks" function allows us to easily identify these peaks and filter extraneous local maxima (some of which can be seen in the figure) by specifying a minimum peak prominence in order to be detected. This function outputs the time (x-position) of each of the peaks. We then average the separation and take the inverse in order to obtain the wave frequency.

We can obtain the velocity with a similar method. If we take our horizontal slice at two relatively close heights, we will see the same pattern of peaks in both graphs, just offset on the x-axis. This offset is the time it took each wave to travel the height. Using the “align signals" function in the MATLAB Signal Processing Toolbox, we can perform cross-correlation to align these signals and obtain their offset. Using the simple slope

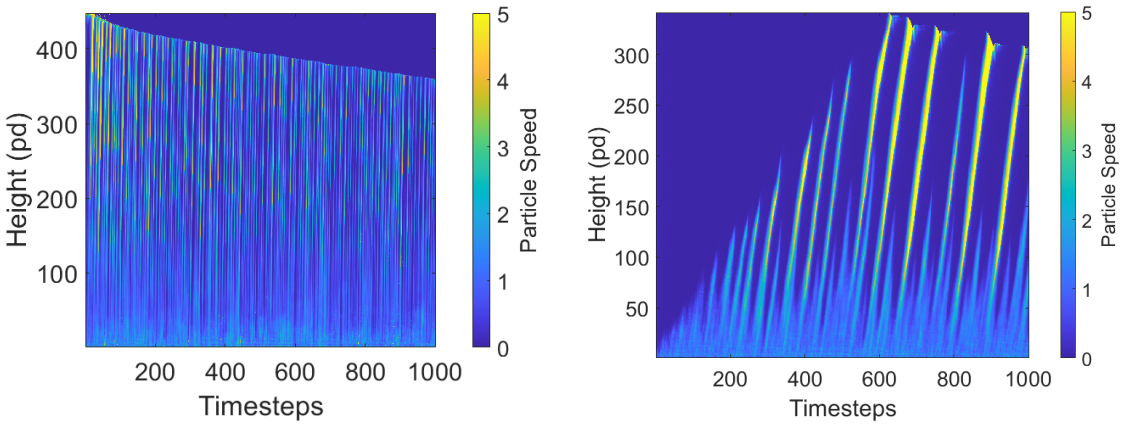

(a) (b)

Figure 5.5: The comparison of two systems with the same gravity, $g = 1$ g and outlet, $D_0 = 11$ pd, but different values of particle stiffness, (a) $E = 10^7$ Pa (b) $E = 10^4$ Pa. Qualitatively, the harder system has far more frequent waves and they appear to have a higher wave speed, i.e. they are more “vertical". The softer system has less frequent waves with a slower wave speed. The softer system also sees more of the waves attenuate before they reach the top of the silo.

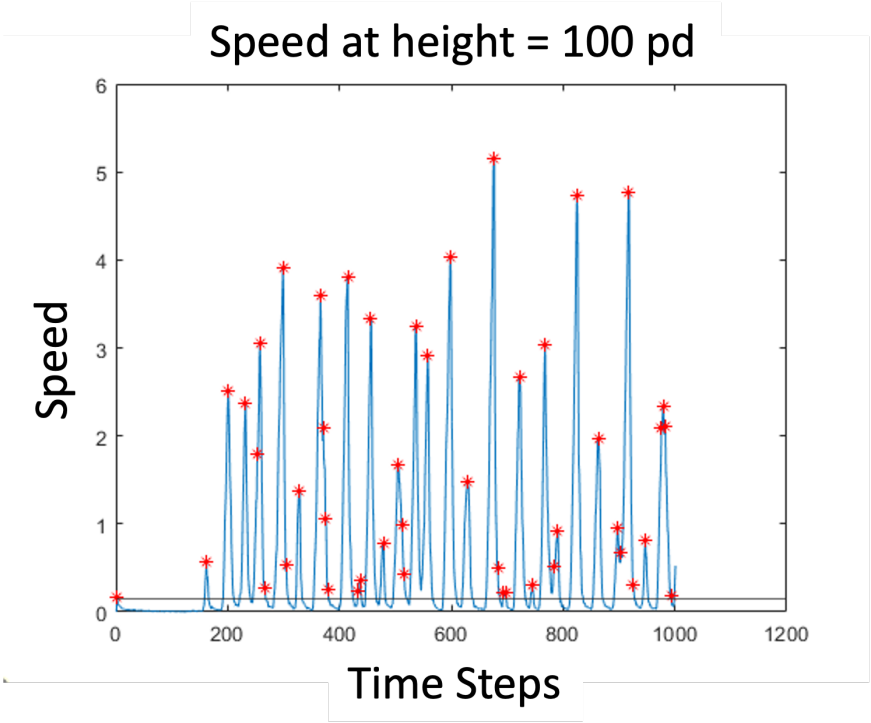

Figure 5.6: Taking a horizontal slice of the spacetime diagram gives us this graph of time steps vs speed. Using the MATLAB “findpeaks" algorithm we identify the pressure waves (red stars).

formula $m = \frac{\Delta y}{\Delta x}$, we can calculate the speed of the wave. Once we have measured the frequency and speed, we can calculate the wavelength from those two measurements.

5.2. Wave Frequency, Speed, and Length Analysis

Figure 5.7 shows the raw data for the measurements of wave speed and frequency. Simulations with the same values of gravity and stiffness did not have significantly different speeds measured as the diameter of the outlet varied. There was more variation observed in in the frequency, but the measurements were still closely clustered. We attempted to normalize both measurements by g and E, but neither normalization was satisfactory, see figure 5.8 for the normalizations for frequency. Because the data varied with

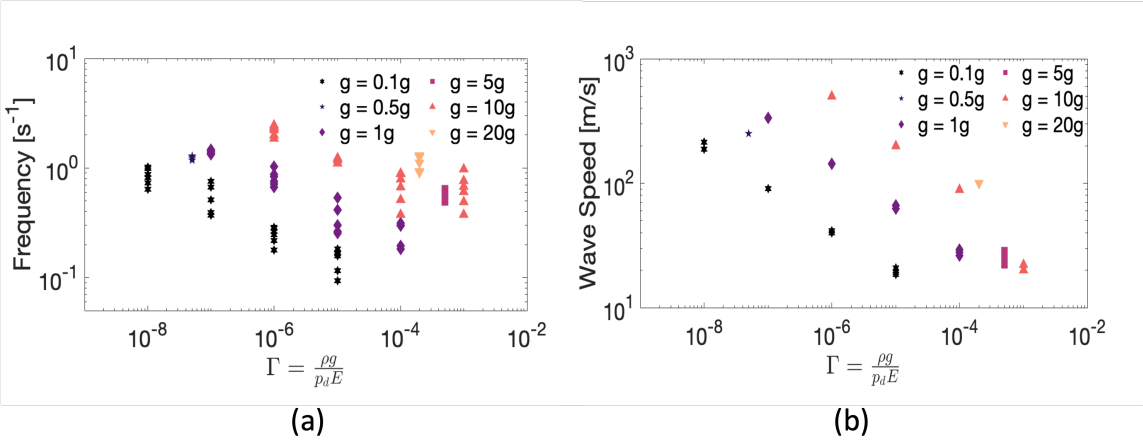

Figure 5.7: Raw data for the (a) wave frequency and (b) wave speed

both g and E, we normalized by Γ, which resulted in the best normalization of the three, although it is not perfect.

Figure 5.10 shows the results for wave speed (a) and frequency (b), normalized by Γ. We fit a -1 power law to the data. At first, it may seem statistically insignificant to fit a fit of Γ^{-1} to the data we divided by Γ, but normalization by Γ reveals an underlying trend in the data that would not occur if it did not depend on it. Figure 5.9 shows an example of what random data normalized by X and fitted by an X^{-1} power law fit does.

The $c \propto \Gamma^{-1}$ fit is interesting, because one might expect the wave speed in the material to be analogous to the speed of sound in the material. The speed of sound is roughly proportional to $\Gamma^{-1/2}$. This means that we are seeing a lower wave speed at high Γ (soft systems and high gravity) than predicted. It is unclear what mechanism(s) drives this difference.

Figure 5.11 shows how frequency and speed depend on gravity and particle stiffness. As mentioned earlier, neither showed a strong dependence on the outlet diameter. We see that both of these measurements have the same trend that we observed qualitatively in the

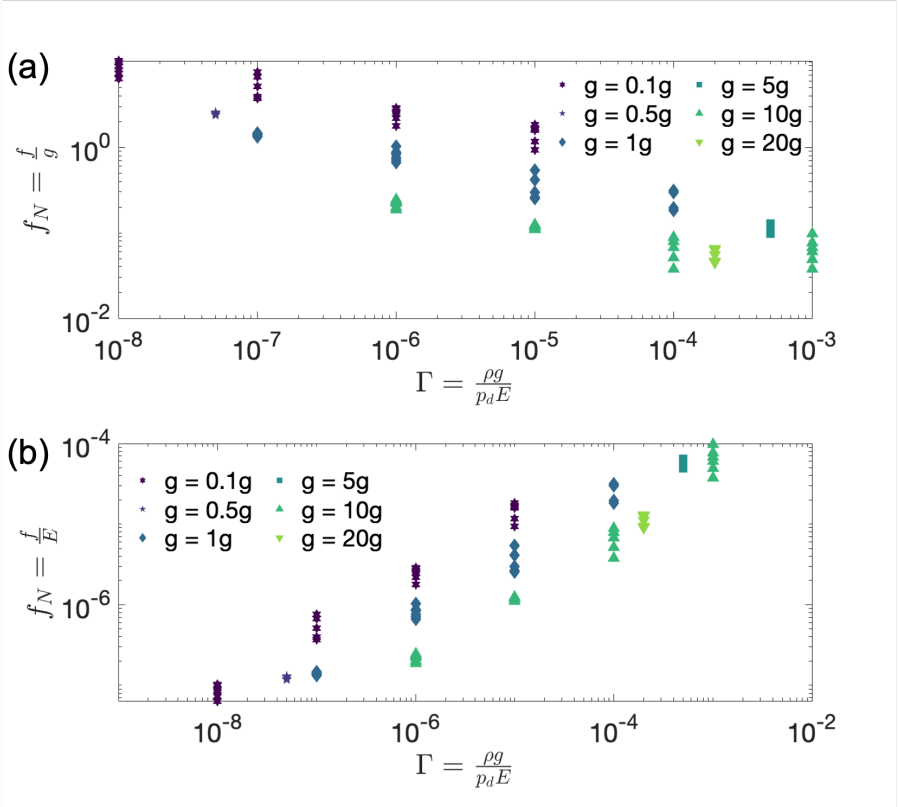

Figure 5.8: Wave frequency normalized by(a) gravity, and (b) Elastic modulus plotted against Γ. Neither of these fits collapses the data as well as Γ.

spacetime diagrams. Softer, higher gravity systems have a lower frequency and slower speed and harder, lower gravity systems have a higher frequency and faster speed.

Because the wavelength is defined as $\lambda = c/f$ and c and f had the same overall relationship to Γ, it could be predicted that the wavelength λ would be constant. However, this does not bear out in the data. Figure 5.12 shows our results for wavelength, plotted against a -1 power law fit. The fit is only for comparison with the other measurements and is not a genuine prediction or fitting attempt. As Γ increases wavelength decreases. The open question is what leads to these different wavelengths within the system.

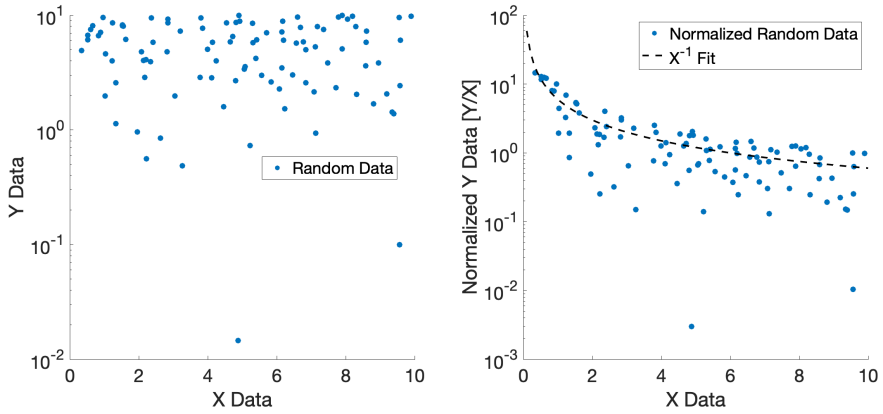

Figure 5.9: Example of random data normalized by its X value fitted by X^{-1}. The data does not collapse to the same extent that our data does in figure 5.10.

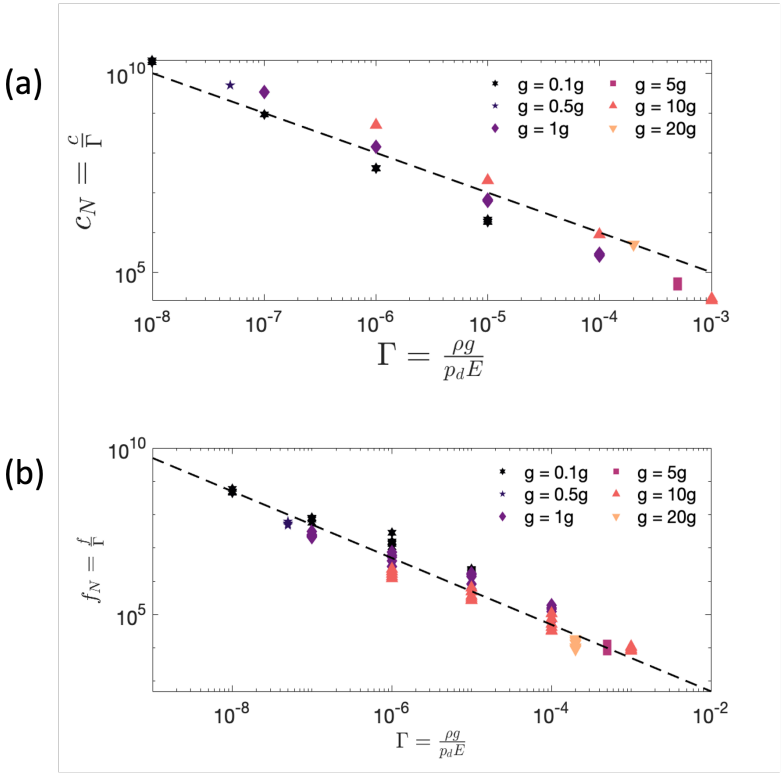

Figure 5.10: (a) Normalized wave speed vs Γ, fitted with a -1 power law fit. (b) Normalized wave frequency vs Γ, also fitted with a -1 power law.

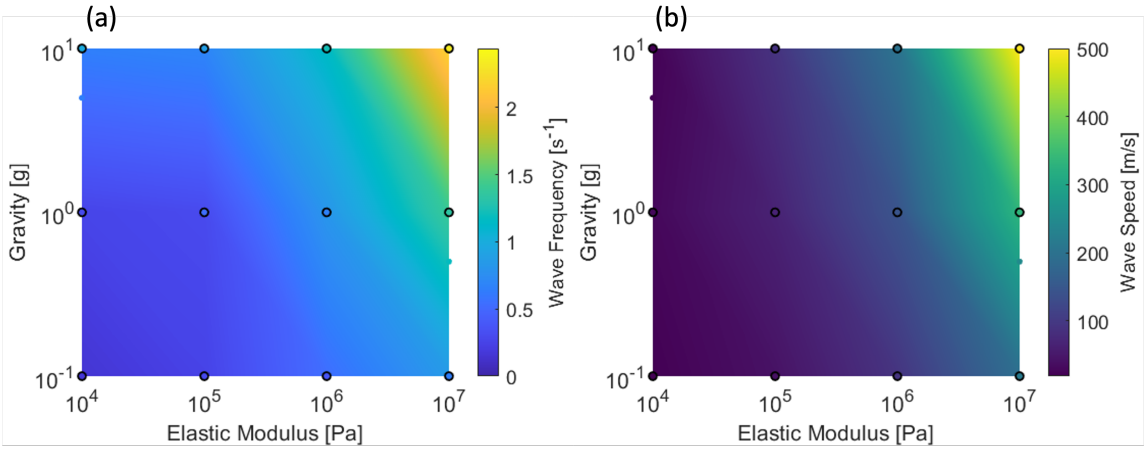

Figure 5.11: Gravity and elastic modulus contour plots of (a) wave frequency and (b) wave speed. The black scatter dots represent the actual data points and the colored background is interpolation.

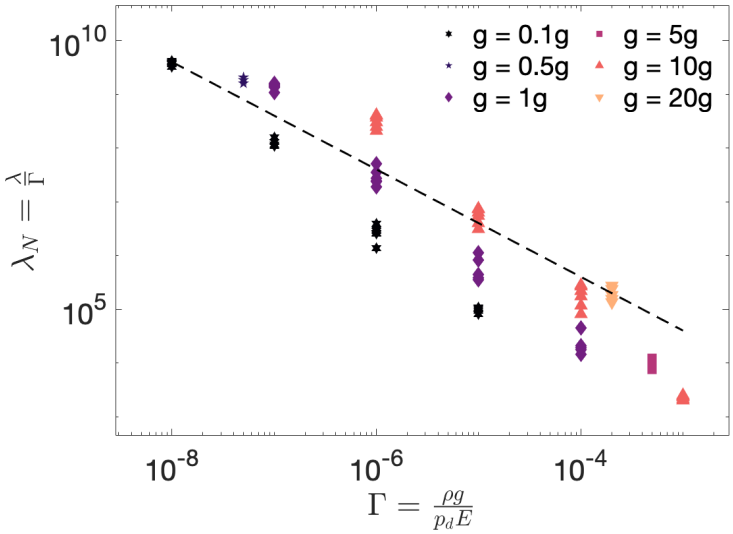

Figure 5.12: Pressure wave wavelength results, plotted with the same -1 power law fit as figures 5.5(a-b).

5.3. Comparison to Flow Rate Fluctuations

Figure 4.9 shows an example of the mass flow of one of our systems over time. While relatively constant, there are fluctuations in the flow. One hypothesis is that the waves are

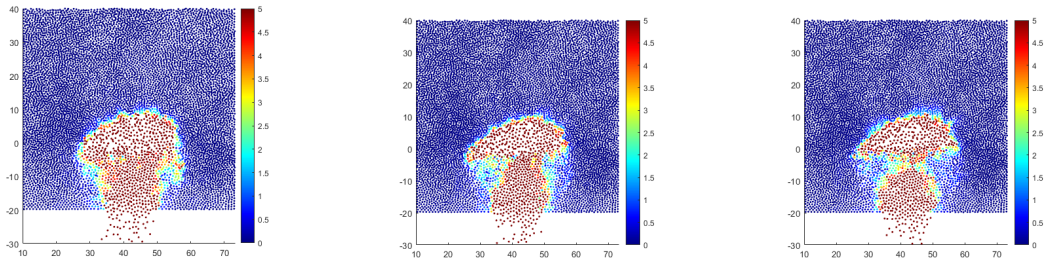

(a) $t = 3.5$s after outlet opened. (b) $t = 3.6$s after outlet opened. (c) $t = 3.7$s after outlet opened.

Figure 5.13: Separation of a pressure wave from the outlet motion in the $E = 10^4$ Pa, $g = 5$g, $D_0 = 15$ pd simulation run. When the low density region widens in (a), particles from the side fall inwards (b), separating the pressure wave from the outlet (c).

correlated with fluctuations in the flow rate. In some videos it appeared that as a void was formed near the outlet, particles along the sides would rush into the empty space, catalyzing the pressure waves (see figure 5.13). We were interested in testing whether there was a relationship between the pressure waves and the flow fluctuations.

We tested this by constructing periodograms of the pressure waves and the flow rate. A periodogram is a signal processing technique that uses fast Fourier transforms to determine the power spectral density (PSD) of a signal. Most real signals, including our pressure wave and flow rate signals, are not comprised of a single frequency. The power of the signal is distributed into many different frequencies. The PSD essentially shows how much of the signal is comprised of each frequency. Figure 5.14 shows the periodograms for the pressure waves and the flow rate (as in figure 4.9). There is clearly a trend in the pressure wave data, although no single frequency dominates. However, for both systems there is no trend in the flow fluctuations. Had both systems showed a peak at the same frequency, we could have determined a relationship between the pressure waves and the flow

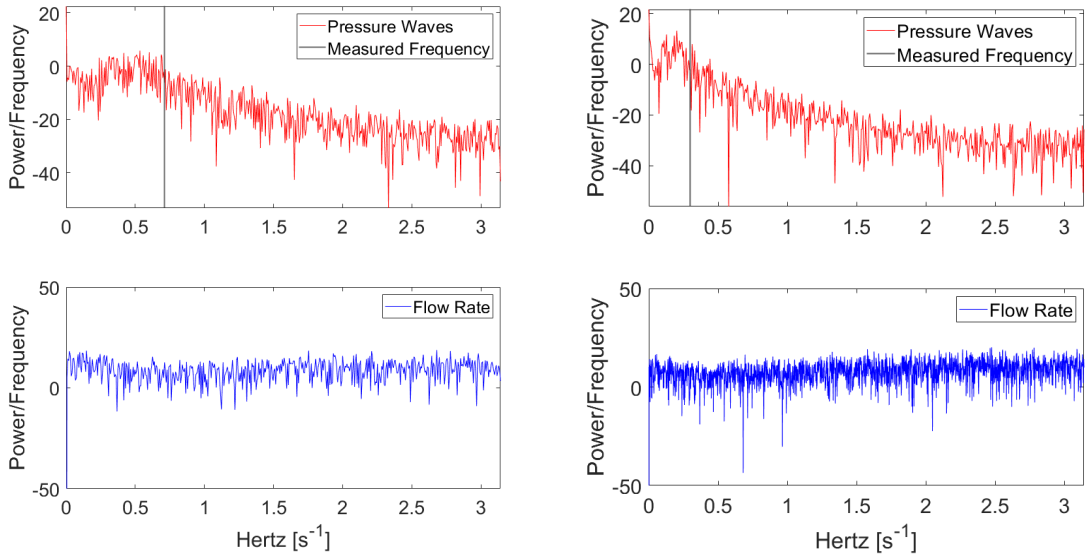

Figure 5.14: Comparison of periodogram of pressure waves and flow rate fluctuations. The pressure wave periodogram for both systems shows a peak with a dominant range of frequencies. No such trend exists in the flow rate. (a) Simulation parameters: $E = 10^6$ Pa, $g = 1$g, $D_0 = 11$ pd. (b) Simulation parameters: $E = 10^4$ Pa, $g = 1$g, $D_0 = 11$ pd.

fluctuations, but no such trend exists. This agrees with previous research that determined that flow variations are random and have no characteristic frequency [32].

6 DISCUSSION AND CONCLUSIONS

Our original goal for this project was to take data at a variety of different gravities and particle stiffnesses in order to look for trends in the bulk, mesoscale, and microscale behaviors. We use the dimensionless constant Γ to do this, which is a ratio of particle density and system gravity to particle stiffness and diameter. We observed that systems with the same value of Γ have the same flow profile, showing the change in the system from a solid-like bulk flow to a fluid-like tunnel flow. Γ also revealed a correlation between flow rate and granular temperature that we believe may be a mechanism behind deviation from the Beverloo prediction. In order to directly compare our results to other research, it will be necessary to convert out of the simulation units. It should be simple to rescale either the mass or length in order to obtain more real-world aligned results.

While our analysis of the pressure waves did not reveal a relationship with fluctuations in the flow rate, it did provide insight into a little-studied aspect of silo flow. Future investigation should look at local rearrangements and the mechanisms behind the formation of the waves. D^2_{min}, a measure of local rearrangements [33], would give insight into this. D^2_{min} is a quantification of how a particle is moving relative to its neighbors. Areas of high D^2_{min} correspond to areas of high plastic deformation, where neighboring particles are moving in different directions. Plastic deformation is simply irreversible deformation of a system, as opposed to elastic deformation, which is reversible. Areas of low D^2_{min} correspond to local affine motion, where the neighboring particles are moving in the same

direction. As it considers local neighborhoods of particles, D^2_{min} is method to analyze the mesoscale of the system.

A weakness of this project is that we ran out of time to analyze local rearrangements. We have a massive amount of data from more than 100 simulations and easily have the ability to run more, if necessary. But because we did not have time to perform local analysis such as D^2_{min}, open questions remain about the pressure waves, granular temperature, and flow rate. A continuation of this project would benefit from performing this analysis. A particularly novel direction for this research would be to use machine learning to explore whether local variations in D^2_{min} can predict bulk behaviors. This method has shown promise in systems under uniform shear [34].

A study of packing structure and its effect on flow should also be performed. As discussed in section 3.4, our systems are very non-crystalline due to our filling method. However, some preliminary simulations used a different filling method and those simulations showed different behavior than the otherwise identical system (most notably a higher flow rate). An interesting question is whether, despite the initial disorder, the system settles into a more crystalline structure during the outflow, as has been found in other systems [33]. Methods to quantify the effect of packing structure include looking at local neighbor count and the $g(r)$ pair correlation function. Local neighbor count is simply a count of particles within a set radius of the reference particle and gives an idea of crystallinity. The $g(r)$ pair correlation function describes the variation of particle number density [35]. $g(r)$ pair correlation is more complex, but gives information on how structurally “solid" or “liquid" a system is. Through these methods a study of packing structure and how it changes over the flow period could be performed.

LITERATURE CITED

[1] H. M. Jaeger, S. R. Nagel, and R. P. Behringer, "Granular solids, liquids, and gases", Reviews of Modern Physics **68**, Publisher: American Physical Society, 1259–1273 (1996).

[2] P. Richard, M. Nicodemi, R. Delannay, P. Ribière, and D. Bideau, "Slow relaxation and compaction of granular systems", en, Nature Materials **4**, 121–128 (2005).

[3] B. Cambou, M. Chaze, and F. Dedecker, "Change of scale in granular materials", en, European Journal of Mechanics - A/Solids **19**, 999–1014 (2000).

[4] N.-S. Nguyen, H. Magoariec, and B. Cambou, "Analysis of local behaviour in granular materials", en, Comptes Rendus Mécanique, Micromechanics of granular materials – A tribute to Ching S. Chang **342**, 156–173 (2014).

[5] R. P. Behringer, D. Bi, B. Chakraborty, A. Clark, J. Dijksman, J. Ren, and J. Zhang, "Statistical properties of granular materials near jamming", en, Journal of Statistical Mechanics: Theory and Experiment **2014**, Publisher: IOP Publishing and SISSA, P06004 (2014).

[6] M. Sperl, "Experiments on corn pressure in silo cells – translation and comment of Janssen's paper from 1895", en, Granular Matter **8**, 59–65 (2006).

[7] C. Mankoc, A. Janda, R. Arévalo, J. M. Pastor, I. Zuriguel, A. Garcimartín, and D. Maza, "The flow rate of granular materials through an orifice", en, Granular Matter **9**, 407–414 (2007).

[8] X. Hong, M. Kohne, M. Morrell, H. Wang, and E. R. Weeks, "Clogging of soft particles in two-dimensional hoppers", Physical Review E **96**, Publisher: American Physical Society, 062605 (2017).

[9] J. C. Mathews and W. Wu, "Model tests of silo discharge in a geotechnical centrifuge", en, Powder Technology, Particle Modelling with the Discrete Element Method A success story of PARDEM (www.pardem.eu) **293**, 3–14 (2016).

[10] S. Dorbolo, L. Maquet, M. Brandenbourger, F. Ludewig, G. Lumay, H. Caps, N. Vandewalle, S. Rondia, M. Mélard, J. van Loon, A. Dowson, and S. Vincent-bonnieu, "Influence of the gravity on the discharge of a silo", English, Granular Matter **15**, Num Pages: 263-273 Place: Heidelberg, Netherlands Publisher: Springer Nature B.V., 263–273 (2013).

[11] A. P. Thompson, H. M. Aktulga, R. Berger, D. S. Bolintineanu, W. M. Brown, P. S. Crozier, P. J. in 't Veld, A. Kohlmeyer, S. G. Moore, T. D. Nguyen, R. Shan, M. J. Stevens, J. Tranchida, C. Trott, and S. J. Plimpton, "LAMMPS - a flexible simulation tool for particle-based materials modeling at the atomic, meso, and continuum scales", en, Computer Physics Communications **271**, 108171 (2022).

[12] I. Zuriguel, A. Garcimartín, D. Maza, L. A. Pugnaloni, and J. M. Pastor, "Jamming during the discharge of granular matter from a silo", Physical Review E **71**, Publisher: American Physical Society, 051303 (2005).

[13] X. Hong, K. W. Desmond, D. Chen, and E. R. Weeks, "Clogging and avalanches in quasi-two-dimensional emulsion hopper flow", Physical Review E **105**, arXiv: 1503.07569, 014603 (2022).

[14] K. Endo, K. A. Reddy, and H. Katsuragi, "Obstacle-shape effect in a two-dimensional granular silo flow field", Physical Review Fluids **2**, arXiv:1706.04791 [cond-mat], 094302 (2017).

[15] R. Nedderman, U. Tüzün, S. Savage, and G. Houlsby, "The flow of granular materials—I", en, Chemical Engineering Science **37**, 1597–1609 (1982).

[16] K. To, P.-Y. Lai, and H. K. Pak, "Jamming of Granular Flow in a Two-Dimensional Hopper", en, Physical Review Letters **86**, 71–74 (2001).

[17] A. Janda, I. Zuriguel, and D. Maza, "Flow Rate of Particles through Apertures Obtained from Self-Similar Density and Velocity Profiles", Physical Review Letters **108**, Publisher: American Physical Society, 248001 (2012).

[18] W. A. Beverloo, H. A. Leniger, and J. van de Velde, "The flow of granular solids through orifices", en, Chemical Engineering Science **15**, 260–269 (1961).

[19] S. M. Rubio-Largo, A. Janda, D. Maza, I. Zuriguel, and R. C. Hidalgo, "Disentangling the Free-Fall Arch Paradox in Silo Discharge", Physical Review Letters **114**, Publisher: American Physical Society, 238002 (2015).

[20] J. Zhang and V. Rudolph, "Effect of shear friction on solid flow through an orifice", Industrial & Engineering Chemistry Research **30**, Publisher: American Chemical Society, 1977–1981 (1991).

[21] T. Pongó, V. Stiga, J. Török, S. Lévay, B. Szabó, R. Stannarius, R. C. Hidalgo, and T. Börzsönyi, "Flow in an hourglass: particle friction and stiffness matter", en, New Journal of Physics **23**, Publisher: IOP Publishing, 023001 (2021).

[22] S. Ogawa, A. Umemura, and N. Oshima, “On the equations of fully fluidized granular materials”, en, Zeitschrift für angewandte Mathematik und Physik ZAMP **31**, 483–493 (1980).

[23] C. S. Campbell, “Rapid Granular Flows”, Annual Review of Fluid Mechanics **22**, _eprint: https://doi.org/10.1146/annurev.fl.22.010190.000421, 57–90 (1990).

[24] T. Börzsönyi and Z. Kovács, “High-speed imaging of traveling waves in a granular material during silo discharge”, en, Physical Review E **83**, 032301 (2011).

[25] N. Bain and D. Bartolo, “Dynamic response and hydrodynamics of polarized crowds”, Science **363**, Publisher: American Association for the Advancement of Science, 46–49 (2019).

[26] M. Moussaïd, D. Helbing, and G. Theraulaz, “How simple rules determine pedestrian behavior and crowd disasters”, Proceedings of the National Academy of Sciences **108**, Publisher: Proceedings of the National Academy of Sciences, 6884–6888 (2011).

[27] L. J. Daniels and D. J. Durian, “Propagating waves in a monolayer of gas-fluidized rods”, en, Physical Review E **83**, 061304 (2011).

[28] Pair_style gran/hooke command — LAMMPS documentation.

[29] L. E. Silbert, D. Ertaş, G. S. Grest, T. C. Halsey, D. Levine, and S. J. Plimpton, “Granular flow down an inclined plane: Bagnold scaling and rheology”, en, Physical Review E **64**, 051302 (2001).

[30] A. Ashour, T. Trittel, T. Börzsönyi, and R. Stannarius, “Silo outflow of soft frictionless spheres”, en, Physical Review Fluids **2**, 123302 (2017).

[31] L. Staron, P.-Y. Lagrée, and S. Popinet, “The granular silo as a continuum plastic flow: The hour-glass vs the clepsydra”, Physics of Fluids **24**, 103301 (2012).

[32] A. Janda, R. Harich, I. Zuriguel, D. Maza, P. Cixous, and A. Garcimartín, “Flow-rate fluctuations in the outpouring of grains from a two-dimensional silo”, en, Physical Review E **79**, 031302 (2009).

[33] D. Chen, D. Semwogerere, J. Sato, V. Breedveld, and E. R. Weeks, “Microscopic structural relaxation in a sheared supercooled colloidal liquid”, Physical Review E **81**, Publisher: American Physical Society, 011403 (2010).

[34] E. D. Cubuk, R. J. S. Ivancic, S. S. Schoenholz, D. J. Strickland, A. Basu, Z. S. Davidson, J. Fontaine, J. L. Hor, Y.-R. Huang, Y. Jiang, N. C. Keim, K. D. Koshigan, J. A. Lefever, T. Liu, X.-G. Ma, D. J. Magagnosc, E. Morrow, C. P. Ortiz, J. M. Rieser, A. Shavit, T. Still, Y. Xu, Y. Zhang, K. N. Nordstrom, P. E. Arratia, R. W. Carpick, D. J. Durian, Z. Fakhraai, D. J. Jerolmack, D. Lee, J. Li, R. Riggleman, K. T. Turner, A. G. Yodh, D. S. Gianola, and A. J. Liu, “Structure-property relationships from universal signatures of plasticity in disordered solids”, Science **358**, Publisher: American Association for the Advancement of Science, 1033–1037 (2017).

[35] C. Liu, Q. Sun, and G. Zhang, “Multiscale properties of dense granular materials”, English, Engineering Computations **32**, Num Pages: 17 Place: Bradford, United Kingdom Publisher: Emerald Group Publishing Limited, 956–972 (2015).

A APPENDICES

A.1. LAMMPS Simulation Code

```
# pour particles into box, settle them,
# create an opening at the bottom and let them run out

# package omp 1

variable name string CAbox_pour20d

thermo_modify flush yes
units  si
variable PI equal 3.141592653589
variable seed equal 14314

################################################
# Geometry-related parameters
################################################

variable xxlo equal 0
variable xxhi equal 21.1
variable yylo equal 0
variable yyhi equal 80
variable zzlo equal -50
variable zzhi equal 650

variable xlo equal 10
variable xhi equal 11.1
variable ylo equal 10
variable yhi equal 73.3
variable zlo equal -20
variable zhi equal 600
variable zhhi equal 450
variable zllo equal -10
```

```
variable yc equal 41.65
variable zc equal 30

variable xcylhi equal 11.1
variable xcyllo equal 10
variable radcyl equal 3

################################################
# Particle sizes
################################################

variable rlo equal 0.5
variable rhi equal 0.5
variable dlo equal 2.0*${rlo}
variable dhi equal 2.0*${rhi}

variable  skin equal ${rhi}
variable rcut equal 2.0*${rhi}

################################################
# Granular contact parameters
################################################

variable coeffRes equal 0.66
variable coeffFric equal 0.5

variable density equal 1
variable EYoung equal 10^4 # original 10^5 (Pa)
variable  Poisson equal 2.0/7.0
variable GShear equal ${EYoung}/(2*(1+${Poisson}))

variable base_gravity equal 9.80665
variable scale equal 0.1
variable gravity equal ${scale}*${base_gravity}

variable reff equal 0.5*(${rhi}+${rlo})
variable meff equal ${density}*4.0/3.0*${PI}*${reff}^3
variable min_mass equal ${density}*4.0/3.0*${PI}*${rlo}*${rlo}*${rlo}
```

```
variable max_mass equal ${density}*4.0/3.0*${PI}*${rhi}*${rhi}*${rhi}

## Typical way to set kn, kt, etc.:
variable        kn equal 4.0*${GShear}/(3*(1-${Poisson}))
variable        kt equal 4.0*${GShear}/(2-${Poisson})

variable a equal (-2.0*log(${coeffRes})/${PI})^2
variable        gamma_n equal sqrt($a*2*${kn}/${min_mass}/(1+0.25*$a))
variable        gamma_t equal ${gamma_n}*0.5

variable tcol equal ${PI}/sqrt(2*${kn}/${min_mass}-${gamma_n}/4.0)
variable ts_scale equal 1
variable dt equal 0.0001 #0.00029831140751*${ts_scale} ${tcol}*0.05
timestep ${dt}

################################################

variable dumpfreq equal 1000*(1/${ts_scale}) #original 10000
variable logfreq equal 1000*(1/${ts_scale})
variable        timecopy atom time
variable        fdir atom (fy^2+fz^2)^0.5
variable        vdir atom (vy^2+vz^2)^0.5

variable        colors string &
                "red green blue yellow white &
                purple pink orange lime gray"

newton  off
atom_style sphere

boundary p p f

region boxreg block ${xxlo} ${xxhi} ${yylo} ${yyhi} ${zzlo} ${zzhi}
create_box 1 boxreg

pair_style gran/hertz/history &
${kn} ${kt} ${gamma_n} ${gamma_t} ${coeffFric} 1
pair_coeff * *
```

```
neighbor        ${skin} bin
thermo  ${logfreq}

comm_style brick
comm_modify  mode multi group all vel yes
balance 1.1 shift xyz 20 1.1
fix bal all balance 10000 1.1 shift xyz 20 1.01

############### Options specific to pouring ##############

# insertion region for fix/pour

region       insreg block ${xlo} ${xhi} ${ylo} ${yhi} ${zllo}
                ${zhhi} side in units box

# defin silo regions - see lammps doc on region command

region      boxxreg block ${xlo} ${xhi} ${ylo} ${yhi} &
${zlo} ${zhi} side in units box

fix ins_grav all gravity ${gravity} vector 0 0 -1
fix 1 all nve/sphere

fix hopper3 all wall/gran/region hertz/history &
        ${kn} ${kt} ${gamma_n} ${gamma_t} ${coeffFric}
        1 region boxxreg


# Create atoms at random positions

create_atoms 1 random 30000 42424 insreg
set type 1 diameter ${dlo} density ${density}


dump 1 all custom ${dumpfreq} ${name}.dump &
x y z vy vz fy fz v_timecopy id
```

```
thermo_style custom step cpu atoms ke
thermo_modify flush yes lost warn

# Initial run to settle the particles

run 600000

# remove "plug" - need to create opening region & union

unfix ins_grav
fix  grav all gravity ${gravity} vector 0 0 -1
region wallreg block ${xlo} ${xhi} 31.65 51.65 &
${zlo} ${zlo} side in units box

region hopreg union 2 boxxreg wallreg

unfix hopper3

fix hopper3 all wall/gran/region hertz/history &
${kn} ${kt} ${gamma_n} ${gamma_t} ${coeffFric} 1 region hopreg

run 5000000
```

A.2. MATLAB LAMMPS Import Code

```
%This program is similar to DumpImporter in that it reads a dump file
%However, this program only pulls from between 2 timesteps defined
%Output is x y z vy vz fy fz time(s) ID timestep
%Author: ATadlock, Last Update: 2020 10 23
%Requires: readdump_pos, readdump_one, a dumpfile and a log file

%==============VARIABLES TO CHANGE=====================
filename = 'CAbox_pour20d.dump';
timesteps =600; %end of insert period
last = 1600;%the last timestep you want
savename = '18d01g10^6'; %name to save matrix under
savefile = 1; % 1 if yes 0 if no
0
%==============BODY=====================
% this gets position data for the end of the settling phase
position = 0;
for i = 1:timesteps
    if rem(i,10)==0 %lists timestep to see progress
        i
    else
    end
    datastr = readdump_pos(filename,position,9);
    position = datastr.position;
end
pos = datastr.position; %position of last timestep of settling

k=1; %k refers to the row
data_2D = nan(30000*(last-timesteps),10); %preallocate space

% get the data for the timesteps we want
for j = timesteps:last
    data_str = readdump_one(filename,pos,9);
    pos = data_str.position;
    atomdata = data_str.atom_data;
    if rem(j,10) == 0
        j
    else
```

```
    end
    if k == 1 %first step only
        data_2D(k:(size(atomdata,1)),1:9) = atomdata;
        data_2D(k:size(atomdata,1),10) = data_str.timestep;
    else
        data_2D(k:(size(atomdata,1)+k-1),1:9) = atomdata;
        data_2D(k:(size(atomdata,1)+k-1),10) = data_str.timestep;
    end
    k = k + 30000;
end

TF = isnan(data_2D(:,1)); %Eliminates NaN rows
data_2D(TF,:) = [];
data_2D = sortrows(data_2D, [10 9]);

if savefile == 1
    save(savename, 'data_2D','-v7.3');
end
```

A.3. Flow Fitting Data

This table contains our flow data. The “Run" column includes Young’s Modulus (E), which is formatted so that 10^4 Pa is 10$\hat{4}$ in the table. D_0 is the outlet width. The flow (W) is in kg/s and the flow deviation is the STD of the data. ρ_b is the bulk density. “Beverloo (minus C)" is $W_0 = \rho_b\sqrt{g}(D_0 - kd_p)^{3/2}$. C is calculated by dividing W/W_0.

Run	D_0	Flow	Flow Deviation	ρ_b	beverloo (minus C)	C
10$\hat{4}$ 1g	7	157.1049	13.0693	5.5896	257.3013765	0.610587095
10$\hat{4}$ 1g	9	226.3293	13.8767	5.5896	396.1413839	0.571334653
10$\hat{4}$ 1g	11	299.3892	15.9861	5.5896	553.6244144	0.540780342
10$\hat{4}$ 1g	15	456.1239	19.3351	5.5896	917.0801376	0.497365368
10$\hat{4}$ 1g	18	587.4137	22.9649	5.5896	1227.124469	0.478691213
10$\hat{4}$ 1g	20	687.2782	8.4367	5.5896	1449.925325	0.474009377
10$\hat{6}$ 1g	6	111.8703	15.5382	4.3283	151.5677714	0.738087649
10$\hat{6}$ 1g	7	145.8884	19.261	4.3283	199.2410097	0.732220742
10$\hat{6}$ 1g	9	216.7593	20.4451	4.3283	306.7516015	0.706628096
10$\hat{6}$ 1g	11	292.2422	25.2382	4.3283	428.6983958	0.681696509
10$\hat{6}$ 1g	15	455.1662	32.3782	4.3283	710.1398954	0.640952864
10$\hat{6}$ 1g	18	577.2491	40.3006	4.3283	950.2223483	0.607488448
10$\hat{6}$ 1g	20	640.6775	42.6904	4.3283	1122.747922	0.570633432
10$\hat{7}$ 10g	6	354.9471	30.3748	4.3091	477.1732429	0.743853737
10$\hat{7}$ 10g	7	454.4203	36.337	4.3091	627.2605175	0.724452261
10$\hat{7}$ 10g	9	678.8802	37.1935	4.3091	965.730743	0.702970476
10$\hat{7}$ 10g	11	917.5143	49.7928	4.3091	1349.649743	0.6798166
10$\hat{7}$ 10g	15	1.43E+03	62.2718	4.3091	2235.697957	6.40E-01
10$\hat{7}$ 10g	18	1.84E+03	75.0362	4.3091	2991.53755	6.17E-01
10$\hat{7}$ 10g	20	2.02E+03	84.3502	4.3091	3534.691193	5.71E-01
10$\hat{6}$ 10g	6	379.699	21.5865	4.6175	511.3242786	0.742579642
10$\hat{6}$ 10g	7	483.6149	23.1857	4.6175	672.1532198	0.719500979
10$\hat{6}$ 10g	9	710.9519	27.2309	4.6175	1034.84758	0.687011222
10$\hat{6}$ 10g	11	949.2052	33.4933	4.6175	1446.243459	0.656324628
10$\hat{6}$ 10g	15	1.48E+03	32.0119	4.6175	2395.705673	6.19E-01
10$\hat{6}$ 10g	18	1.93E+03	48.6006	4.6175	3205.640305	6.01E-01
10$\hat{6}$ 10g	20	2.22E+03	50.0734	4.6175	3787.667166	5.85E-01

Run	D_0	Flow	Flow Deviation	ρ_b	beverloo (minus C)	C
10$\hat{7}$ 1g	6	101.6311	23.4568	4.23	148.1255165	0.686114739
10$\hat{7}$ 1g	7	133.9567	27.9714	4.23	194.7160481	0.687959217
10$\hat{7}$ 1g	9	200.0465	34.4591	4.23	299.7849674	0.667299971
10$\hat{7}$ 1g	11	274.2177	47.0012	4.23	418.9622286	0.65451652
10$\hat{7}$ 1g	15	399.2044	70.0419	4.23	694.0119118	0.575212605
10$\hat{7}$ 1g	18	506.2513	80.6729	4.23	928.6418533	0.545152362
10$\hat{7}$ 1g	20	583.8243	85.4029	4.23	1097.249199	0.532079951
10$\hat{4}$ 0.1g	6	37.7414	6.1462	4.606	51.00508126	0.739953727
10$\hat{4}$ 0.1g	7	48.9538	7.2957	4.606	67.04792053	0.730131518
10$\hat{4}$ 0.1g	9	72.7749	7.1704	4.606	103.2270266	0.704998511
10$\hat{4}$ 0.1g	11	94.7344	8.809	4.606	144.2641553	0.656673169
10$\hat{4}$ 0.1g	15	148.6386	11.1848	4.606	238.9739108	0.621986724
10$\hat{4}$ 0.1g	18	195.4428	11.5743	4.606	319.7656577	0.611206348
10$\hat{4}$ 0.1g	20	222.3943	13.1586	4.606	377.8233886	0.588619727
10$\hat{5}$ 0.1g	6	36.1911	7.496	4.319	47.8269531	0.756709296
10$\hat{5}$ 0.1g	7	46.2861	7.6332	4.319	62.87016256	0.736217279
10$\hat{5}$ 0.1g	9	67.7746	9.8799	4.319	96.79494741	0.700187374
10$\hat{5}$ 0.1g	11	90.059	12.8039	4.319	135.2750514	0.665747298
10$\hat{5}$ 0.1g	15	144.5551	15.5993	4.319	224.0834391	0.645094972
10$\hat{5}$ 0.1g	18	185.8892	17.1802	4.319	299.8410498	0.619959142
10$\hat{5}$ 0.1g	20	205.3682	19.8981	4.319	354.2812017	0.57967569
10$\hat{5}$ 1g	6	120.2902	12.7368	4.6189	161.7439593	0.743707527
10$\hat{5}$ 1g	7	155.6199	13.8715	4.6189	212.6179562	0.73192266
10$\hat{5}$ 1g	9	227.8871	13.3795	4.6189	327.3467579	0.696164219
10$\hat{5}$ 1g	11	299.3081	15.4576	4.6189	457.4810018	0.654252524
10$\hat{5}$ 1g	15			4.6189	757.8183497	0
10$\hat{5}$ 1g	18	607.4191	22.2117	4.6189	1014.019824	0.599020932
10$\hat{5}$ 1g	20	712.4455	24.2091	4.6189	1198.128682	0.594631871
10$\hat{6}$ 0.1g	6	34.145	8.6585	4.2688	47.27105751	0.722323591
10$\hat{6}$ 0.1g	7	43.7919	11.2631	4.2688	62.13941884	0.704736234
10$\hat{6}$ 0.1g	9	63.2127	15.2807	4.2688	95.66989385	0.660737641
10$\hat{6}$ 0.1g	11	81.4064	22.2469	4.2688	133.7027413	0.608861114
10$\hat{6}$ 0.1g	15	135.5645	23.1407	4.2688	221.4789037	0.612087642
10$\hat{6}$ 0.1g	18	171.4865	27.0858	4.2688	296.3559791	0.57865038
10$\hat{6}$ 0.1g	20	172.5782	33.7051	4.2688	350.1633698	0.492850523
10$\hat{7}$ .1g	5	23.9787	3.1132	4.2494	33.67069682	0.712153364
10$\hat{7}$ .1g	6	30.5183	3.5608	4.2494	47.05622933	0.648549627
10$\hat{7}$ .1g	7	42.7	4.1834	4.2494	61.85701987	0.690301603
10$\hat{7}$ .1g	9	56.9334	5.087	4.2494	95.23511219	0.597819425
10$\hat{7}$ .1g	11	77.4071	5.7374	4.2494	133.0951154	0.581592343
10$\hat{7}$ .1g	15	114.1659	7.462	4.2494	220.4723701	0.51782407

Run	D_0	Flow	Flow Deviation	ρ_b	beverloo (minus C)	C
10$\hat{7}$ .1g	18	143.3165	8.563	4.2494	295.0091589	0.485803561
10$\hat{7}$ .1g	20	132.7905	8.4079	4.2494	348.5720164	0.38095571
10$\hat{7}$ .5g	5	51.7615	4.1	4.2389	75.10393016	0.689198287
10$\hat{7}$ .5g	6	73.0474	4.7694	4.2389	104.9609333	0.695948461
10$\hat{7}$ .5g	7	93.6066	5.3151	4.2389	137.9747299	0.678432928
10$\hat{7}$ .5g	9	142.5044	6.3453	4.2389	212.4259933	0.670842574
10$\hat{7}$ .5g	11	188.2818	7.232	4.2389	296.8743507	0.634213766
10$\hat{7}$ .5g	15	283.0425	9.6816	4.2389	491.7730564	0.575555119
10$\hat{7}$ .5g	18	352.756	11.5126	4.2389	658.0305536	0.536078451
10$\hat{7}$ .5g	20	348.0983	12.5955	4.2389	777.5047994	0.447712092
10$\hat{5}$ 10g	5	289.0265	6.1048	5.6965	451.3698979	0.640331802
10$\hat{5}$ 10g	6	394.9858	6.3491	5.6965	630.8086092	0.626157909
10$\hat{5}$ 10g	7	499.6628	6.8141	5.6965	829.2194514	0.602570042
10$\hat{5}$ 10g	9	714.2315	7.781	5.6965	1276.666863	0.559450175
10$\hat{5}$ 10g	11	947.809	8.5394	5.6965	1784.196181	0.531224655
10$\hat{5}$ 10g	15	1.44E+03	1.05E+01	5.6965	2955.525147	4.88E-01
10$\hat{5}$ 10g	18	1.86E+03	1.24E+01	5.6965	3954.722251	4.70E-01
10$\hat{5}$ 10g	20	2.14E+03	1.32E+01	5.6965	4672.754957	4.59E-01
10$\hat{5}$ 20g	5	427.855	7.0347	6.6615	746.4685601	0.573172164
10$\hat{5}$ 20g	6	576.0869	7.4085	6.6615	1043.221527	0.552219145
10$\hat{5}$ 20g	7	724.105	7.8532	6.6615	1371.350311	0.528023361
10$\hat{5}$ 20g	9	1.03E+03	8.63E+00	6.6615	2111.331923	0.49
10$\hat{5}$ 20g	11	1.35E+03	9.48E+00	6.6615	2950.676064	0.46
10$\hat{5}$ 20g	15	2.04E+03	1.18E+01	6.6615	4887.801803	0.42
10$\hat{5}$ 20g	18	2.60E+03	1.39E+01	6.6615	6540.258529	0.40
10$\hat{5}$ 20g	20	2.99E+03	1.66E+01	6.6615	7727.729918	0.39
10$\hat{4}$ 5g	5	231.3566	5.644	10.5064	588.6585063	0.39
10$\hat{4}$ 5g	6	311.6206	6.1816	10.5064	822.6752723	0.38
10$\hat{4}$ 5g	7	393.9578	6.8838	10.5064	1081.43473	0.36
10$\hat{4}$ 5g	9	556.3052	7.2519	10.5064	1664.977686	0.33
10$\hat{4}$ 5g	11	743.724	8.5779	10.5064	2326.877055	0.32
10$\hat{4}$ 5g	15	1.13E+03	10.7237	10.5064	3854.477285	0.29
10$\hat{4}$ 5g	18	1.43E+03	12.5356	10.5064	5157.590048	0.28
10$\hat{4}$ 5g	20	1.64E+03	13.5777	10.5064	6094.019486	0.27
10$\hat{4}$ 10g	5	373.3152	7.2667	15.9201	1261.4507	0.30
10$\hat{4}$ 10g	6	488.6352	7.4886	15.9201	1762.930947	0.28
10$\hat{4}$ 10g	7	616.1796	8.1084	15.9201	2317.432913	0.27
10$\hat{4}$ 10g	9	886.2283	10.1592	15.9201	3567.921376	0.25
10$\hat{4}$ 10g	11	1.17E+03	12.3607	15.9201	4986.32171	0.23
10$\hat{4}$ 10g	15	1.81E+03	23.0514	15.9201	8259.853576	0.22
10$\hat{4}$ 10g	18	2.33E+03	32.846	15.9201	11052.32576	0.21
10$\hat{4}$ 10g	20	2.74E+03	36.4284	15.9201	13059.02329	0.21